THE PREPARATION AND CHARACTERIZATION OF ZEOLITE CONFINED RHODIUM(0) NANOCLUSTERS: A HETEROGENEOUS CATALYST FOR THE HYDROGEN GENERATION FROM THE METHANOLYSIS OF AMMONIA-BORANE

A THESIS SUBMITTED TO
THE GRADUATE SCHOOL OF NATURAL AND APPLIED SCIENCES
OF
MIDDLE EAST TECHNICAL UNIVERSITY

BY

SALİM ÇALIŞKAN

IN PARTIAL FULFILLMENT OF THE REQUIREMENTS
FOR
THE DEGREE OF MASTER OF SCIENCE
IN
CHEMISTRY

MARCH 2010

Approval of the thesis:

THE PREPARATION AND CHARACTERIZATION OF ZEOLITE CONFINED RHODIUM(0) NANOCLUSTERS: A HETEROGENEOUS CATALYST FOR THE HYDROGEN GENERATION FROM THE METHANOLYSIS OF AMMONIA-BORANE

submitted by **SALİM ÇALIŞKAN** in partial fulfillment of the requirements for the degree of **Master of Science in Chemistry Department, Middle East Technical University** by,

Prof. Dr. Canan Özgen
Dean, Graduate School of **Natural and Applied Sciences** _____

Prof. Dr. İlker Özkan
Head of Department, **Chemistry, METU** _____

Prof. Dr. Saim Özkar
Supervisor, **Chemistry Department, METU** _____

Examining Committee Members:

Prof. Dr. Zuhal Küçükyavuz _____
Chemistry Dept., METU

Prof. Dr. Saim Özkar _____
Chemistry Dept., METU

Prof. Dr. Gülsün Gökağaç _____
Chemistry Dept., METU

Prof. Dr. İnci Eroğlu _____
Chemical Engineering Dept., METU

Assoc. Prof. Dr. Ayşen Yılmaz _____
Chemistry Dept., METU

Date: March 30, 2010

I hereby declare that all information in this document has been obtained and presented in accordance with academic rules and ethical conduct. I also declare that, as required by these rules and conduct, I have fully cited and referenced all material and results that are not original to this work.

Name, Last name: Salim Çalışkan

Signature:

ABSTRACT

THE PREPARATION AND CHARACTERIZATION OF ZEOLITE CONFINED RHODIUM(0) NANOCLUSTERS: A HETEROGENEOUS CATALYST FOR THE HYDROGEN GENERATION FROM THE METHANOLYSIS OF AMMONIA-BORANE

Çalışkan, Salim

M.Sc., Department of Chemistry

Supervisor: Prof. Dr. Saim Özkar

March 2010, 73 pages

Among the new hydrogen storage materials, ammonia borane (AB) appears to be the most promising one as it has high hydrogen content, high stability, and being environmentally benign. Dehydrogenation of AB can be achieved via hydrolysis, thermolysis or methanolysis. Methanolysis of AB eliminates some drawbacks of other dehydrogenation reactions of AB. The use of colloidal and supported particles as more active catalyst than their bulky counterparts for the hydrolysis of AB implies that reducing the particle size can cause an increase in the catalytic activity as the fraction of the surface atoms increases by decreasing the particle size. Similarly, transition metal nanoclusters can be utilized as catalyst for the methanolysis of AB as well. For this purpose transition metal nanoclusters need to be stabilized to a certain extent. Actually in the catalytic application of transition metal nanoclusters one of the most important problems is the aggregation of nanoclusters into bulk metal, despite of using the best stabilizers. In this regards, the use of metal nanoclusters as catalysts in systems with confined void spaces such as inside mesoporous and microporous solids appears to be an efficient way of preventing aggregation.

In this dissertation we report for the first time the use of intrazeolite rhodium(0) nanoclusters as a catalyst in the methanolysis of ammonia borane. Rhodium(0) nanoclusters could be generated in zeolite-Y by a two-step procedure: (*i)* incorporation of rhodium(III) cations into the zeolite-Y by ion-exchange, (*ii*) reduction of rhodium(III) ions within the zeolite cages by sodium borohydride in aqueous solution, followed by filtration and dehydration by heating to 550 °C under 10^{-4} Torr. Zeolite confined rhodium(0) nanoclusters are stable enough to be isolated as solid materials and characterized by ICP-OES, XRD, SEM, EDX, HRTEM, XPS and N_2 adsorption-desorption technique. The zeolite confined rhodium(0) nanoclusters are isolable, bottleable, redispersible and reusable. They are active catalyst in the methanolysis of ammonia-borane even at low temperatures. They provide exceptional catalytic activity with an average value of TOF = 380 h^{-1} and unprecedented lifetime with 74300 turnovers in the methanolysis of ammonia-borane at 25 ± 0.1 °C. The work reported here also includes the full experimental details of previously unavailable kinetic data to determine the rate law, and activation parameters (E_a, $\Delta H^{\neq}$ and $\Delta S^{\neq}$) for the catalytic methanolysis of ammonia-borane.

Keywords: Ammonia borane, Rhodium(0) nanoclusters, Zeolite, Methanolysis, Hydrogen, Heterogeneous catalysis

ÖZ

ZEOLİT İÇERİSİNE HAPSEDİLMİŞ RODYUM(0) NANOKÜMELERİNİN HAZIRLANMASI VE TANIMLANMASI: AMONYAK-BORANIN METANOLİZ TEPKİMESİNDEN HİDROJEN ÜRETİMİ İÇİN HETEROJEN KATALİZÖR

Çalışkan, Salim

Yüksek Lisans, Kimya Bölümü

Tez Yöneticisi: Prof. Dr. Saim Özkar

Mart 2010, 73 sayfa

Yeni hidrojen depolama malzemeleri içerisinde; yüksek hidrojen kapasitesi, yüksek kararlılığı ve çevreye zararsız oluşuyla, amonyak boran en çok gelecek vaadedendir. Amonyak boranın dehidrojenasyonu hidroliz, termoliz veya metanoliz yoluyla gerçekleştirilebilir. Amonyak boranın metanolizi diğer dehidrojenasyon reaksiyonlarının bazı eksikliklerini gidermektedir. Kolloidal ve destekli parçaçıkların külçe muadillerine oranla daha aktif katalizör olarak amonyak boranın hidrolizinde kullanılması parçacık boyutunu küçülttükçe yüzey atomları oranı artacağından parçacık boyutu küçüldükçe katalitik aktivitede yükselme olacağını belirtmektedir. Benzer biçimde, geçiş metal nanokümeleri amonyak boranın metanolizinde de katalizör olarak kullanılabilir. Bu amaçla, geçiş metal nanokümelerinin belirli bir ölçüye kadar kararlaştırılması gerekir. Geçiş metal nanokümelerinin katalitik uygulamalarında en önemli problemlerden biri en iyi kararlaştırıcılar kullanılmasına rağmen nanokümelerin külçe metale topaklanmasıdır. Bu bakımdan, metal nanokümelerin katalizör olarak mikrogözenekli ve mezogözenekli katılar gibi sınırlandırılmış boş hacimli sistemler ile kullanılması topaklanmayı önleyecek etkili bir biçimdir.

Bu tezde ilk kez intrazeolit rodyum(0) nanokümelerinin amonyak boranın metanolizinde katalizör olarak kullanımını sunuyoruz. Rodyum(0) nanokümeleri zeolit-Y içerisinde iki basamaklı bir prosedür ile hazırlanabildi: (i) rodyum(III) katyonlarının zeolit-Y içerisine iyon-değişimi ile sokulması, (ii) rodyum(III) katyonlarının zeolit içinde sodyum borhidrür ile indirgenmesi, takiben süzme ve 10^{-4} Torr altında 550 ^{0}C'ye kadar ısıtılma. Zeolit içerisine hapsedilmiş rodyum(0) nanokümeleri katı malzeme olarak izole edildi ve ICP-OES, XRD, SEM, EDX, HRTEM, XPS ve N_2 adsorpsiyon-desorpsiyon teknikleri ile karakterize edildi. Zeolit içerisine hapsedilmiş rodyum(0) nanokümeleri izole edilebilir, şişelenebilir, tekrar dağılabilir ve tekrar kullanılabilir. Zeolit içerisine hapsedilmiş rodyum(0)nanokümeleri amonyak boranın metanolizinde düşük sıcaklıklarda bile aktif bir katalizördür. Burada sunulan çalışma, amonyak boranın metanolizinde hız denklemi ve aktivasyon parametrelerinin (E_a, $\Delta H^{\neq}$ and $\Delta S^{\neq}$) hesaplanması için daha önce mevcut olmayan kinetik bilgilerin bütün deneysel detaylarını içermektedir. Ortalama TOF=380 h^{-1} değeri ve daha önce görülmemiş 74300 toplam çevrim sayısı ile amonyak boranın 25 ± 0.1 °C'de AB'nin metanolizinde olağanüstü katalitik aktivite göstermektedir.

Anahtar Sözcükler: Amonyak boran, Rodyum(0) nanokümeleri, Zeolit, Metanoliz, Hidrojen, Heterojen katalizör.

To My Family…

ACKNOWLEDGEMENTS

I would like to express my deepest gratitude to my supervisor Prof. Dr. Saim Özkar. Starting from the first day, he responded me very politely and always encouraged me with his positive attitude. I sincerely appreciate the time and efforts he has taken to train me and improve my thesis.

I wish to acknowledge Mehmet Zahmakıran. First for his endless friendship and brotherhood. Then, I am also respectful to him since; he gave me advices before the experiments, spared his time to help me during the experiments and also encouraged me if I felt lazy.

I also give my special thanks to Dr. Feyyaz Durap, from Chemistry Department of Dicle University, for his great friendship and encouragement during my study.

I sincerely acknowledge my friends; Hüseyin Özgür Gündüz, Özer Candarlı, Muhammet Emre Yurttagül, Serdar Akbayrak, and Fırat Hacıoğlu with whom I had spent most of time after working hours when preparing my thesis.

I am also thankful to my laboratory friends from Organometallics and Nanoclusters Research Group for their patience and politeness during my study.

I am also thankful to Chemistry Department of Middle East Technical University for providing facilities used in this study.

I am also thankful to members of Karamanoğlu Mehmetbey University for their support and patience during this study.

The last but not least, I would like to extend my gratitude to my family for their endless love and support in every step of my life. I could not achieve any of these without their support and belief in me.

TABLE OF CONTENTS

LIST OF TABLES

TABLES

LIST OF FIGURES

FIGURES

CHAPTER 1

INTRODUCTION

1.1. Hydrogen Economy

One of the most important challenges in global economy is the energy problem. Since energy is the key sector in social and economic development worlds leading countries invest much on new strategies towards solving the energy problem [1]. World's energy production mostly based on combustion of fossil fuels. However using fossil fuels as an energy source has two major hurdles to be overcomed: *(i)* depletion of fossil fuel sources within next decades [2,3] and *(ii)* global environmental problems related to fossil fuels and their combustion products. The challenge lies in finding a way to harmonize the necessity and demand for energy supply with its impact on the natural resource base in order to ensure a sustainable path of development.

On the road to approaching sustainable energy future, hydrogen based energy technologies are today a major topic of international importance for energy supply and environmental protection. Hydrogen economy refers to a vision of the future in which electric power will be generated not by direct combustion of fossil fuels or by nuclear fission, but by electrochemical oxidation of hydrogen in a fuel cell device [4].

Hydrogen is regarded as a perfect energy carrier due to its unique charateristics. These features were described by Sherif: ‘’ *(i)* it can be produced from and converted into electricity at relatively high efficiencies, *(ii)* its raw material for production is water, which is available in abundance, *(iii)* it is a completely renewable fuel, *(iv)* it can be stored in gaseous form (convenient for large-scale storage), in liquid form (convenient for air and space transportation), or in the form of metal hydrides (convenient for surface vehicles and other relatively small-scale storage requirements), *(v)* it can be transported over large distances through pipelines or via tankers, *(vi)* it can be converted into other forms of energy in more ways and more efficiently than any other fuel (such as catalytic combustion, electrochemical conversion, and hydriding), *(vii)* it is environmentally compatible since its production, storage, transportation, and end use do not produce any pollutants (except for small amounts of nitrogen oxides), greenhouse gases, or any other harmful effects on the environment ‘’ [5].

Despite the unique features of hydrogen those make it as an ideal energy carrier, there are still some struggles concerning production, storage and transportation technologies of hydrogen. Though its high abundancy (hydrogen is the nineth most plentiful element in the Earth, about 0.9 percentage by weight of the Earth’s surface is hydrogen [6]) and simplicity, it is difficult to find elemental hydrogen on Earth, it is always found as combined with other elements. Today several methods are being used to produce hydrogen: *(i)* production of hydrogen by water electrolysis [7], *(ii)* direct thermal decomposition of water [8], *(iii)* thermochemical cycles [9], *(iv)* photolysis [10] and *(v)* hydrogen production from biomass [11].

Due to its low density (gasoline density is 0.7 kg/L whilst H_2 density is 0.03, 0.06 and 0.07 kg/L at 350 atm, 700 atm and liquefied (20 K), respectively [12]) storage of hydrogen in compressed or liquid form is too difficult; therefore large amounts of hydrogen storage is still a big challenge in hydrogen economy.

There are several storing technologies used depending on the storage size and application. Hydrogen storage technologies can be mainly examined into four groups [4]: *(i)* compressed gas, *(ii)* cryogenic liquid, *(iii)* metal hydrides, and *(iv)* chemical hydrides.

In a hydrogen economy, another important and struggled issue is the transportation of hydrogen. From the production plants and/or storage, hydrogen should be transported safely to the consumers. It is likely that hydrogen will be transmitted to consumers by means of underground pipelines (gaseous hydrogen) and/or supertankers (liquid hydrogen) [5].

Production, storage and transportation technologies of hydrogen are commercially accesible today. But still there are struggles concerning economy and feasibility. According to scientists two conditions must be met in order to have a society based on hydrogen economy [12]. Firstly international organizations must guarantee the fulfilment of the international agreements on global reductions in CO_2 emissions. Unless this condition is met, fossil fuels will continue to dominate the energy scenario for decades. Secondly the costs of production, storage, transportation and utilization of hydrogen must be reduced with the technological improvements. If these major hurdles mentioned above will be somehow overcomed; than hydrogen will become the basic energy infrastructure that will power the next generations, replacing today's natural gas, oil, coal, and electricity infrastructures in the world.

1.2. Ammonia Borane as a Prominent Hydrogen Storage Material

As mentioned previously; storage and transport of hydrogen are the most challenging technological barriers to be overcomed in hydrogen economy. Since hydrogen is the lightest of all elements (density: 0.08988 gL^{-1}) in the periodic table, it is too difficult to store hydrogen in the gas form [13].

The storage of hydrogen at high pressures or at vey low temperatures is not economically easy and is not practically safe. In this regards chemical hydrogen storage is a convenient way to store hydrogen especially for on-board applications. Several kinds of solid materials such as metal/complex hydrides [14], metal nitride and imides [15], carbon nanotubes [16], TiO_2 nanotubes [17], and metal-organic frameworks [18] have been tested for hydrogen storage. Ammonia borane (H_3NBH_3, AB) and amine borane compounds have recently attracted researchers as being promising candidates for chemical hydrogen storage material. Amongst the new hydrogen storage materials, AB appears to be be outstanding nominee for hydrogen storage [19]. AB has a low molecular weight (30.9 g/mol) and has the highest hydrogen content (19.6 wt %) [20], that is greater than the 2015 target of U.S. Department of Energy (9 wt. % for a material to be applicable). AB is solid at room ambient temperatures due to it is being strongly polar molecule and having strong intermolecular interactions based on different electronegativities of B and N atoms. AB is nontoxic, stable at ambient temperatures, environmentally harmless, readly available and can be handled at room temperature. AB is thermally stable enough to transport and store. AB is stable in air and aqueous solutions and in absence of catalysts or protic solvents there is no liberation of hydrogen observed. AB can release hydrogen via thermolysis [21], hydrolysis [22], and methanolysis [23].

Despite of wide usage of AB in various reactions, still two major problems must be eliminated before using AB in practical applications: (*i*) developing efficient and economical catalysts to enhance the kinetic and thermodynamic properties under moderate conditions and (*ii*) reversibility of the reactions should be achieved. Recently, Ramachandran and co-workers showed that the use of methanol instead of water can overcome problem of liberation of ammonia gas and that they achieved the recyling of methanolysis product to ammonia-borane with high yields (81 %) and purity (98%) [23].

$$NH_3BH_3 + 4MeOH \xrightarrow{\text{catalyst}} NH_4B(OMe)_4 + 3H_2 \qquad (1)$$

Methanolysis of AB (Equation 1) eliminates some drawbacks of other dehydrogenation reactions of AB. Hydrolysis of high concentrations of AB can liberate ammonia (NH_3) gas which can cause problems in fuel cell applications. Unlike hydrolysis, methanolysis of AB does not liberate NH_3. Moreover the product of hydrolysis is not recyclable, on the other hand the methanolysis product tetrametoxyborate can be recyclable and via methanolysis of AB an efficient recyclable hydrogen generation system is achieved as shown in Figure 1.1.

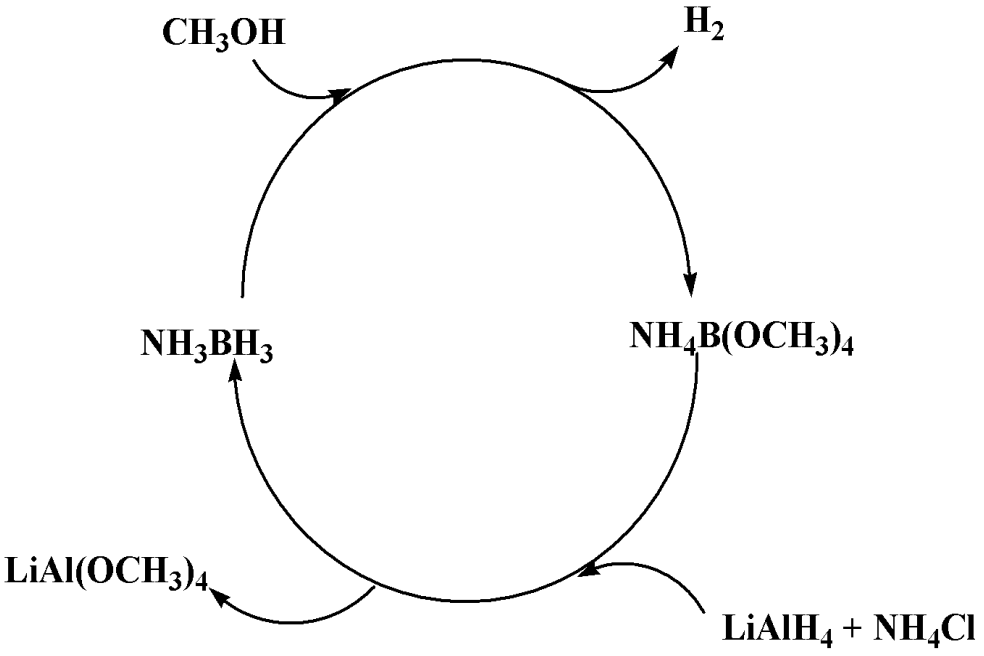

Figure 1.1. Ammonia-borane hydrogen cycle (adopted from literature [23]).

Methanolysis of AB occurs only in the presence of a suitable catalyst. So far, various kinds of transition metal catalysts have been tested in methanolysis of AB: $RuCl_3$, $RhCl_3$, $CoCl_2$, $NiCl_2$, Pd/C, Raney Ni, and Co-Co_2B, Ni-Ni_3B, Co-Ni-B [23]. However all the reports lack information about the lifetime of the catalyst. Among all the highest catalytic activity has been achieved with $RuCl_3$, with a TOF value 173 min^{-1}. However, since the sole stabilizer present in the system is the weakly coordinating chloride anion which cannot provide enough stabilization for the rhodium(0) nanoclusters, aggregation of rhodium(0) particles occur. This study has clearly shown that *(i)* in the methanolysis of AB, reducing the particle size of heterogeneous catalyst can provide a significant increase in its activity as the fraction of surface atoms increases with the decreasing particle size, *(ii)* transition metal nanocluster catalysts need to be stabilized to certain extend. Even using the best stabilizers still aggregation problem can occur in catalytic application of transition metal nanoclusters. The use of metal nanoclusters as catalysts in systems with confined void spaces such as inside mesoporous and microporous solids appears to be an efficient way of preventing aggregation. In this regards, we used zeolite confined rhodium(0) nanoclusters as highly active and long lived catalyst for the methanolysis of AB.

CHAPTER 2

TRANSITION METAL NANOCLUSTERS IN CATALYSIS

2.1. Key Definitions in Catalysis

Catalysis is defined as the ability of substances to awaken affinities, which are asleep at a particular temperature, by their mere presence and not by their own affinity. Catalysts are substances that accompany a catalytic process by increasing the rate of reaction without themselves undergoing any change thereby. During the reaction it may come to existence in a different entity but at the end of the reaction, it returns to the same as the start.

Catalysts fall into three main groups as: Heterogeneous, Homogeneous, and Biological. General classification of catalysts is given in Figure 2.1.

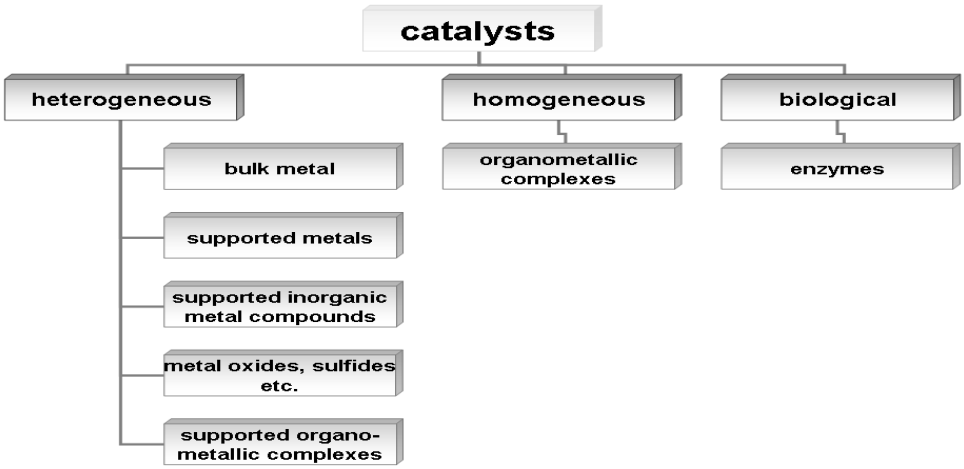

Figure 2.1. Classification of catalysts

Homogeneous and heterogeneous classification is depending on whether it exists in the same phase as the substrate. Homogeneous catalyst acts in same phase with the substrates. Heterogeneous catalysts are those that act in different phase than substrates. Heterogeneous catalysis is crucial to chemical technology. Most catalytic processes are heterogeneous in nature, typically involving a solid catalyst and gas- or liquid-phase reactants. The majority of the industrial processes involve heterogeneous catalysis. Table 2.1 illustrates some common heterogeneous catalytic processes.

Table 2.1. Examples of industrial processes that use heterogeneous catalysts (adopted from literature [24]).

Industrial Manufacturing Process	**Catalyst System**
NH_3 synthesis (Haber process)	Fe on SiO_2 and Al_2O_3 support
Water – gas shift reaction	Ni, iron oxides
Catalytic cracking of heavy petroleum distillates	Zeolites
Catalytic reforming of hydrocarbons to improve octane number	Pt, Pt-Ir and other Pt-group metals on acidic alumina support
Methanation	Ni on support
Ethene epoxidation	Ag on support
HNO_3 manufacture (Haber – Bosch process)	Pt-Rh gauzes

Heterogeneous catalysts are easily separated from the reaction products. They are stable, and easier to prepare, handle, recover, and re-use. They also have low cost and low toxicity. However heterogeneous catalysts often tend to require high temperatures and pressures, and selectivity is lower compared to homogeneous catalysts. Two advantages of homogeneous catalysts over heterogeneous catalysts are: having relatively mild conditions (require low T and low P) and higher selectivity. On the other hand, the need to separate the catalyst at the end of the reaction, in order to recycle it, is more difficult than heterogeneous one.

There also exist another group of catalysts those cannot be categorized according to phase difference: Biocatalysts which are also called enzymes. Enzymes possess the highest level of complexity among the three types of catalysts. Enzymes are nature's own catalysts and fundamental for life, as they catalyze essentially all biological processes.

Whatever the type of catalyst is, a reaction is not usually catalyzed by only the uniqueness of a species. Moreover a number of criteria must be considered when choosing the most effective and suitable catalyst. The criterias those should be considered are; *(i)* the concentration of catalyst, *(ii)* the catalytic turnover, *(iii)* the selectivity of the catalyst to the desired product, *(iv)* size of the catalyst and *(v)* catalytic lifetime of the catalyst.

A catalytic reaction is one in which more than one turnover or event occurs per reaction center or catalytically active site; which means that the turnover number is greater than 1. Thus a reaction is not catalytic if it is stoichiometric or if its turnover number (TON) is less than 1. In catalysis, the catalytic turnover number (TON) is defined as the number of moles of product per mole of catalyst, which also gives the number of catalytic cycles for a given process. The catalytic turnover frequency (TOF) is defined as number of revolutions of the catalytic cycle per unit time, generally the second.

For a given reaction catalyzed by Q, the rate of the reaction equation, the turnover frequency and the turnover number can be given by the following equations.

$$A \xrightarrow{Q} B \qquad v = \frac{d[B]}{dt} \qquad (1)$$

$$TON = \frac{[B]}{[Q]} = \frac{\text{moles of product}}{\text{moles of catalyst}} \qquad (2)$$

$$TOF = \frac{v}{[Q]} = \frac{\text{moles of product}}{\text{moles of catalyst x time}} \qquad (3)$$

Equally significant with the catalytic efficiency; selectivity is one of the challenges in catalysis area. Whether it is homogeneous or heterogeneous; one of the most important roles of catalysts is shifting the reaction towards getting better selectivity to a desired product in a chemical reaction that leads to more than one product normally. A good selective catalyst yields a high proportion of the desired product with minimum amount of the side products. High selectivity plays a key role in industry to reduce waste, to reduce the work-up equipment of a plant, and to ensure a more effective use of the feedstocks.

2.2. Free Energy Profile

Chemical bonds are broken and new chemical bonds are formed during the catalytic process. But during these processes most important thing is the lowering of activation energy of a catalyst. A catalyst changes the activation energy of a

reaction in two ways. In the first way, it forms bonds with one or more of the reactants and so reduces the energy needed by the reactant molecules in order to complete the reaction. In the second way, it brings the reactants together and holds them in a way that makes reaction more likely. When molecules come together in the appropriate orientation for reaction there is a big reduction in entropy. If a catalyst already holds the molecules next to each other then the entropy change for the reaction step will be far less negative than it would be without the catalyst, and the reaction is more likely. As a result; the reaction becomes faster than the uncatalyzed one. Note that the catalyst does not affect the overall entropy change for the reaction. Catalysts increase the rate of approach to equilibrium but not the thermodynamic equilibrium value itself. In other words a catalyst provides a new reaction pathway with a low barrier of activation, which may involve many intermediates and many steps. The sequence of steps we call the mechanism of the reaction. The uncatalyzed reaction has higher activation energy than that of any catalyzed reaction. The differences in activation energies between catalyzed and uncatalyzed reactions are shown in Figure 2.3.

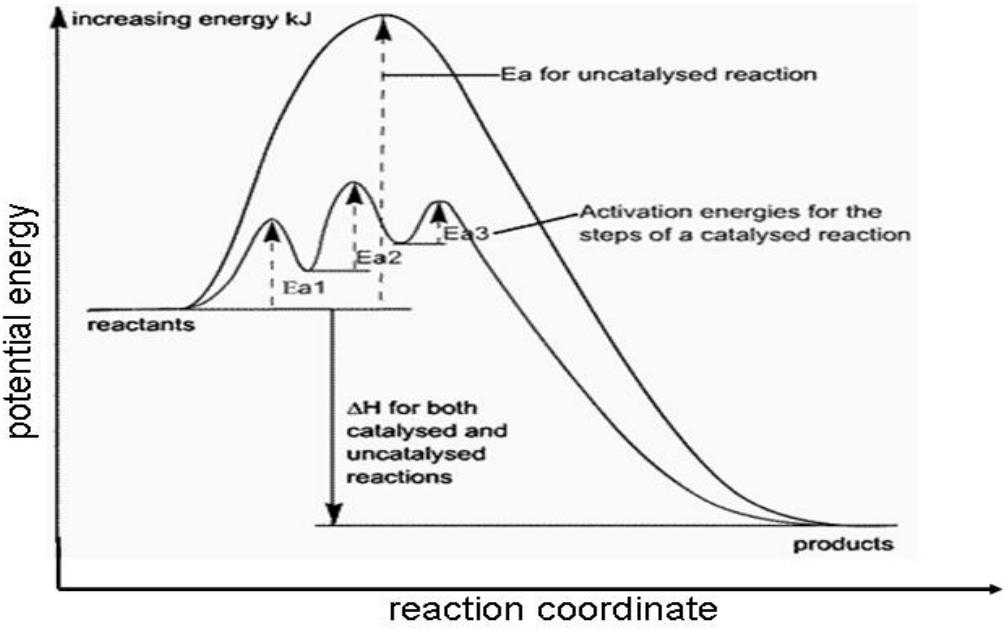

Figure 2.2. Schematic representation of the energetics in a catalytic cycle.

2.2. Effect of Size Reduction of Catalysts

Bulk gold is known as one of the most inert metals in the periodic table. This property is because lacking of interaction between surface and reactant [25]. Year 1989 is a milestone in reactivity of gold particles that Haruta and coworkers demonstrated that Au nanoclusters (<10 nm) dispersed on TiO_2 support displayed unexpectedly high activity toward CO oxidation [26] and propylene epoxidation [27]. When metal clusters are only a few atomic layers thick, the size of clusters and surface structure of the oxide can have significant impact on the chemisorptive properties of the metal. Since the investigation of exceptional reactivity of gold nanoparticles in catalysis, researchers try to picturize surface property and surface chemistry of nanoparticles [28].

Surface processes are of key importance in multifarious processes, including corrosion, adsorption, oxidation-reduction and catalysis. Understanding the surface properties and surface chemistry of nanoparticles is essential if nanoparticle behavior is to be fully understood. From macroscale to nanoscale there exists a considerable change in the intrinsic properties of materials; moreover the properties of nanoparticles also change with size. Band gaps can change, coercive force in magnetic materials can be manipulated, melting points can decrease with size, surfaces can be more reactive, and nanostructural metal specimens can have increased hardness by a factor [29].

Nanoscale particles exhibit unusual surface morphologies and possess more reactive surfaces, hereby open a new perspective in surface chemistry. Metal nanoparticles show a great potential catalysis because of the large surface area of these particles. The huge surface areas of the nanostructured material dictate that many of the atoms lie on the surface, thus allowing good ‘atom economy’ in surface-gas, surface-liquid, or even surface-solid reactions. Nanoclusters have a high percentage of their metal atoms on the surface, 50% of the metal atoms are on the surface of a 2.0-nm nanoclusters [30]. Moreover surface atoms in

nanoclusters do not necessarily order themselves in the same way that those in bulk do. Klabunde et al calculate the numbers of iron atoms on spherical iron nanoclusters that are surface or bulk atoms which is illustrated in Figure 2.3 [31].

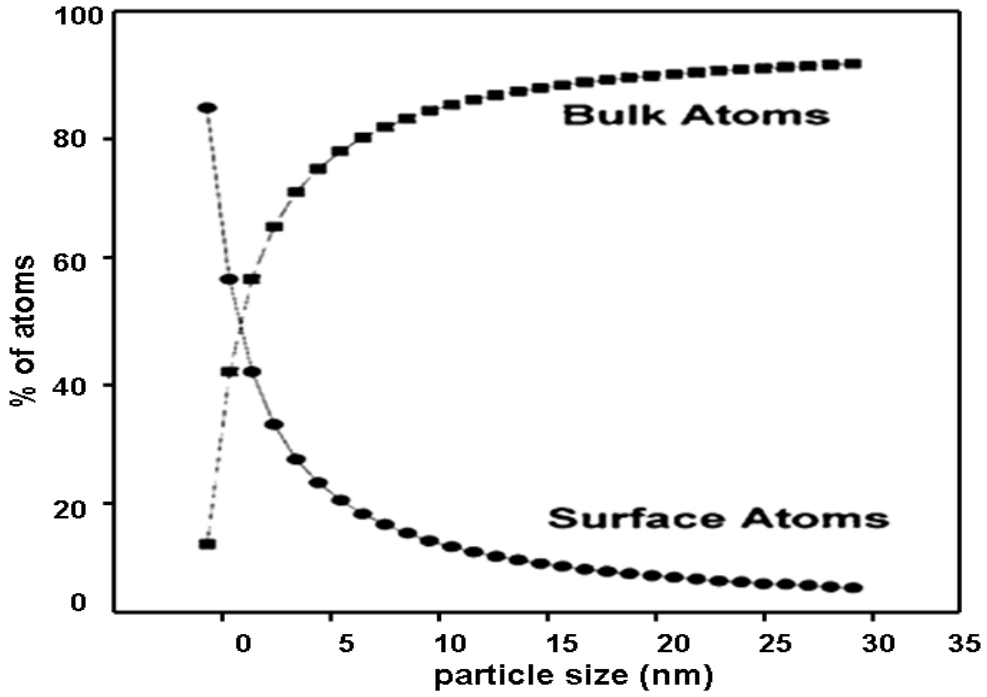

Figure 2.3. Calculated surface to bulk ratios for solid metal particles versus size (adopted from the literature [31])

2.4. Transition Metal Nanoclusters

Transition metal nanoclusters are near-monodisperse (≤15% size dispersion) particles that are generally less than 10 nm [32]. The size, shape, size distribution and composition of transition metal nanoclusters can be controlled by reproducible syntheses [33]. They have unique properties coming from the fact that these particles and their properties lie somewhere between those of bulk and single-particle species [34]. Other important features of the nanoclusters are that

they are stable enough to be isolable, bottleable, and fully redissolvable yet they retain high catalytic activity and long lifetime when redissolved in nonaqueous solvents [33].

They are currently in particular interest due to wide variety applications including quantum dots [35], quantum computers [36], quantum devices [37], chemical sensors [38], photochemistry [39], nanoelectronics [40], light-emitting diodes [41], ferrofluids for cell separations [42], photochemical pattern applications [43]. Supporting information to these claims, a recent review states, '' Metal nanoparticles are certain to be the building blocks of the next generation of electronic, optoelectronic, and chemical sensing devices'' [44].

Transition metal nanoclusters have significant roles in catalysis as being highly active and selective catalysts then their bulky counterparts. The reasons that transition metal nanoclusers are more active and selective catalysts than their bulk counterparts can be described as; (*i*) a large precentage of nanoclusters' metal atoms lie on the surface, (*ii*) surface atoms do not necessarily order themselves in the same way that those in bulk do, (*iii*) the electrons in nanocluster are confined to spaces that can be as small as a few atom widths giving rise to quantum size effect, (*iv*) nanoclusters offer the possibility of controlling the nanocluster size in a quantitative and modifiable way.

Transition metal nanoclusters are widely used in different catalytic applications such as; catalytic reforming reactions [45], hydrocracking and aromitization processes [46], hydrogenations [47], hydrosilyations [48], oxidation of alcohols [49], McMurry [50], Suzuki [51], Heck-type couplings [52] and cycloaddition reactions [53].

2.4.1. Synthesis of Transition Metal Nanoclusters

There are several methods of synthesizing transition metal nanoclusters. These methods can be divided into two methods: physical methods, also known as top-down, and chemical methods, also known as bottom-up [54]. The physical method, also called as top-down, is proceed by the mechanical grinding of bulk metals and subsequent stabilization of the resulting nanosized metal particles by the addition of colloidal protecting agents [55].

Chemical methods are the most convenient way of synthesizing of transition metal nanoclusters since controlling the size of nanoclusters is easy. In general these methods can be divided into four main categories as: *(i)* reduction of transition metal salt precursors, *(ii)* electrochemical synthesis, *(iii)* organometallic synthesis, *(iv)* metal vapor synthesis. And other less common methods are redox surface techniques [56], thermal [57] and photochemical [58] decomposition of metal complex precursors, sonochemical synthesis [59] and laser ablation.

2.4.2. Stabilization of Metal Nanoclusters

Despite the fact that transition metal nanoclusters are very active catalysts then their counter bulk particles, there is an important problem that leads aggregation of transition metal nanoclusters into bulk material. By aggregation, transition metal nanoclusters lose their properties such as losing their activity. Nanoclusters are only kinetically stable; therefore in order to prevent aggregation into larger particles and to have resultant nanoclusters that are stable enough to be isolable, bottleable, and fully redissolvable yet retain high catalytic activity and long lifetime when redissolved in nonaqueous solvents; stabilization of metal nanoclusters is important.

Stabilization of metal nanoparticles can be accomplished by four ways: *(i)* electrostatic stabilization, *(ii)* steric stabilization, *(iii)* electrosteric stabilization, and *(iv)* stabilization by a ligand or solvent.

2.4.2.1. Electrostatic Stabilization

In 1940s, B. Derjaguin, L. Landau, E. Verway, and J.T.G. Overbeek developed the theory for the general electrostatic stabilization mechanisms of colloidal materials known as DLVO theory [60]. According to this theory; nanocluster stabilization is based on a fragile balance in interparticle forces between repulsive Coulombic forces opposing attractive van der Waals forces. The adsorption of ions to the electrophilic metal surface generates an electrical double-layer around the metal nanoparticles resulting a Coulombic repulsion between particles (Figure 2.4). Moreover a case study on electrostatic stabilization, acetate stabilized Ru(0) nanoclusters, is given in Figure 2.4.

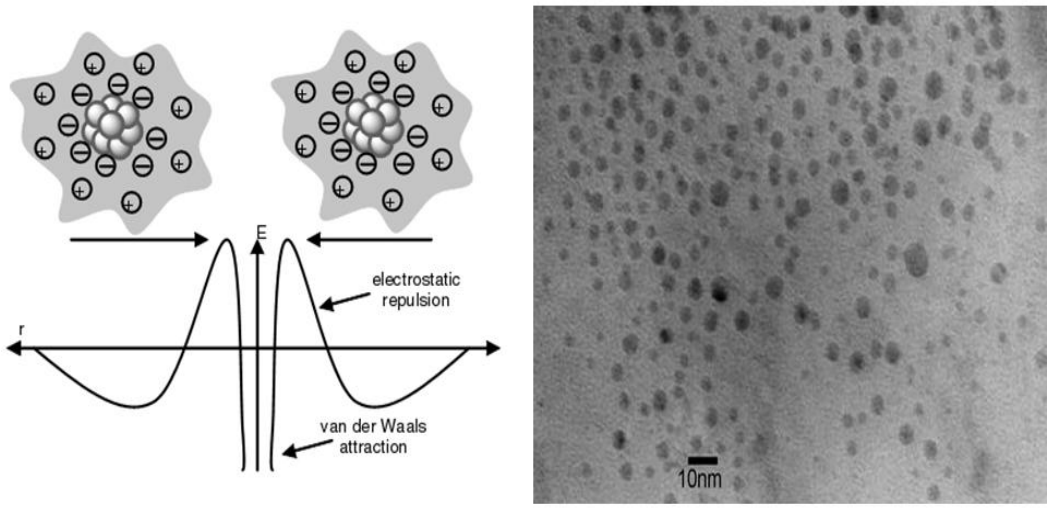

Figure 2.4. (a) Schematic representation of electrostatic stabilization, (b) Acetate stabilized Ru(0) nanoclusters (adopted from literature [61]).

2.4.2.2. Steric Stabilization

In this type of stabilization, aggregation into bulk material is prevented by surrounding metal clusters by sterically bulky macromolecules such as polymers [62] or surfactants [63]. The adsorption of these large molecules onto metal surface will create a steric protective barrier that impedes diffusing of metal particle centers. Schematic representation of steric stabilization and a case study, PVP stabilized Ni(0) nanoclusters, are given in Figure 2.5.

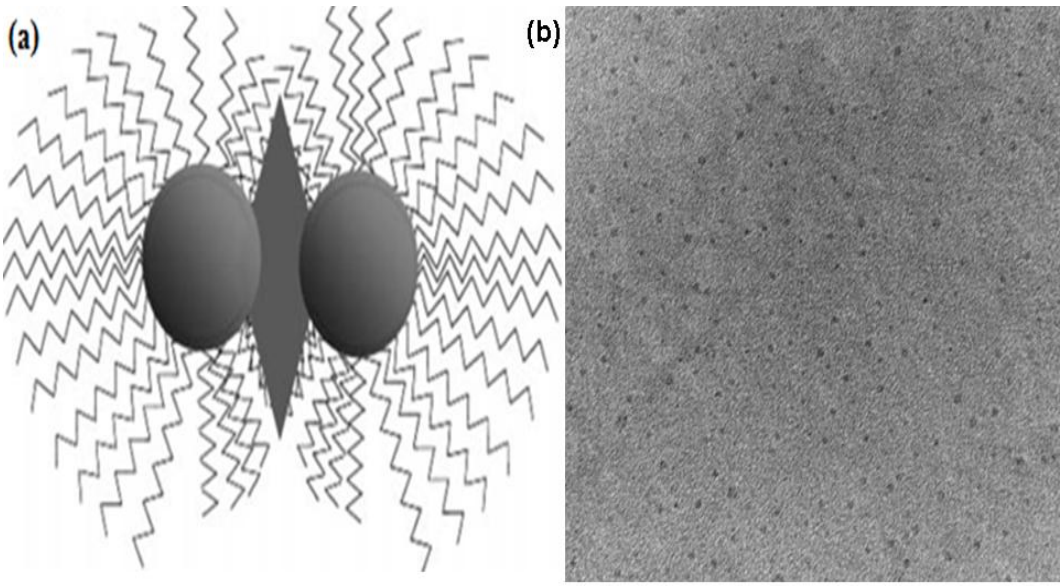

Figure 2.5. (a) Schematic representation of steric stabilization, (b) PVP stabilized Ni(0) nanoclusters (adopted from literature [64]).

2.4.2.3. Electrosteric Stabilization

Combination of electrostatic and steric stabilization is so-called electrosteric stabilization. Electrosteric stabilizers used in this type of stabilization are generally ionic surfactants. These stabilizers generate an electrical double layer by their polar head groups and they provide steric repulsion by their side chains. When two particles approach each other, both electrostatic repulsion and steric restriction would prevent agglomeration. In Figure 2.6 electrosteric stabilization is picturized and one case study by Ozkar, polyoxoanions stabilized Ir(0) nanoclusters, is given.

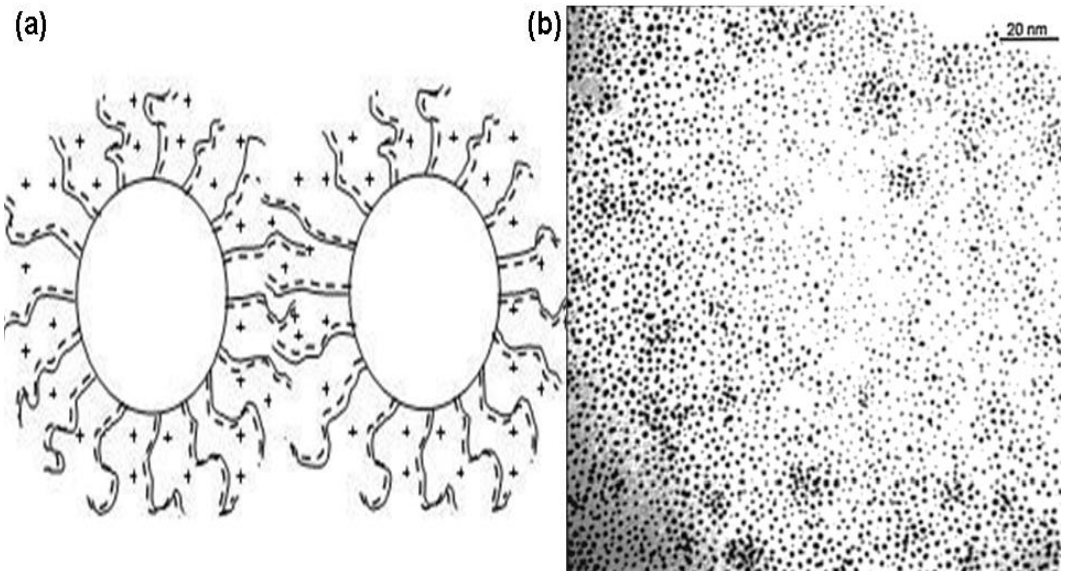

Figure 2.6. (a) Schematic representation of electrosteric stabilization (b) Polyoxoanions stabilized Ir(0) nanoclusters (adopted from literature [65])

2.4.2.4. Stabilization by a Ligand or Solvent

In this case traditional ligands are used to stabilize transition metal particles. Metal nanoparticles are coordinated to the traditional ligands such as phosphines [66], thiols [67], amines [68], carbon monoxide [69].

2.4.2.5. Encapsulation of Transition Metal Nanoclusters in Confined Void Spaces Provides an Alternative Way for Their Stabilization

In the catalytic application of transition metal nanoclusters one of the most important problems is the aggregation of nanoclusters into clumps and ultimately to bulk metal, despite of using the best stabilizers [33]. The use of metal nanoclusters as catalysts in systems with confined void spaces such as inside mesoporous and microporous solids appears to be an efficient way of preventing aggregation [70]. From this point of view, zeolite type minerals are considered to be suitable host materials for catalytic applications. Especially Faujasite zeolites, including X and Y type zeolite, which possess large cavities known as supercages within their structures, have been used for the preparation of metal nanoparticles such as Rh, Ru, Pd, Pt, Au, Ag and Cu [71,23].

2.4.2.5.1. Zeolites

Zeolites occur in nature and have been known as aluminosilicate minerals. Zeolites are aluminosilicates with framework structures providing cavities occupied by large ions and water molecules, both of which have considerable freedom of movement, permitting ion-exchange and reversible dehydration [72]. The framework structure consists of corner-linked tetrahedral in which small atoms lie at the centers of tetrahedra and oxygen atoms lie at the corners.

The elementary building units for zeolites are SiO_4 and AlO_4 tetrahedra. The zeolite composition can be best described as having three components:

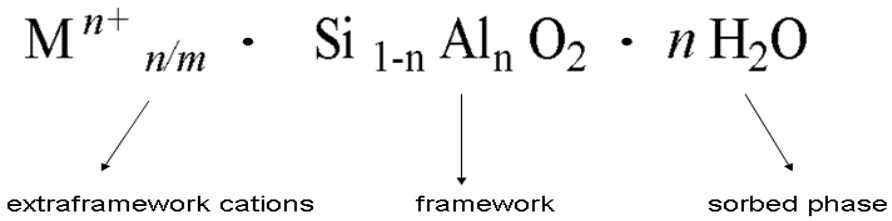

Figure 2.7. Composition of a typical zeolite

Adjacent tetrahedra are linked at their corners via a common oxygen atom, and this result in an inorganic macromolecule with a structurally distinct three-dimensional framework. The framework of a zeolite contains channels, channel intersections and/or cages with dimensions from 0.2 to 1 nm. Figure 2.11 shows the structures of four selected zeolites along with their respective void systems and pore dimensions.

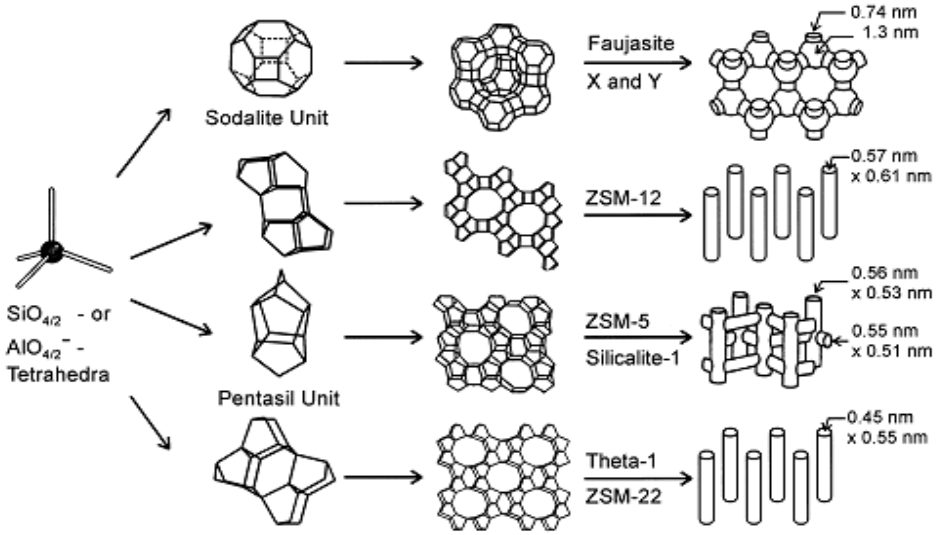

Figure 2.8. Structures of four selected zeolites and their micropore systems and dimensions (adopted from literature [73]).

Zeolites offer unique opportunities for studies of heterogeneous catalysis because of their catalytic, structural, and ion-exchange properties: *(i)* the strictly regular pore size and pore architecture, *(ii)* pore widths of molecular dimensions which enable shape or size selective catalysis, *(iii)* acidic properties which can be tuned by various methods, *(iv)* the various possibilities for changing the zeolite properties by ion-exchange, dealumination/realumination and isomorphous substitution, *(v)* the high thermal stability with the possibility to regenerate deactivated catalysts, *(vi)* the capability of zeolites to act as hosts or carriers for a variety of guests having catalytic activity, e.g., transition metal ions, complexes or chelates, basic alkali metal or metal oxide clusters and enzymes.

As mentioned previously, zeolite-Y is considered as a suitable host providing highly ordered large cavities (supercages) with a diameter of 1.3 nm [71]. Its pore system is relatively spacious and consists of spherical cages, referred to as supercages, with a diameter of 1.3 nm connected tetrahedrally with four neighboring cages through windows with a 4 diameter of 0.74 nm. The three dimensional structure of zeolite-Y is given in Figure 2.9.

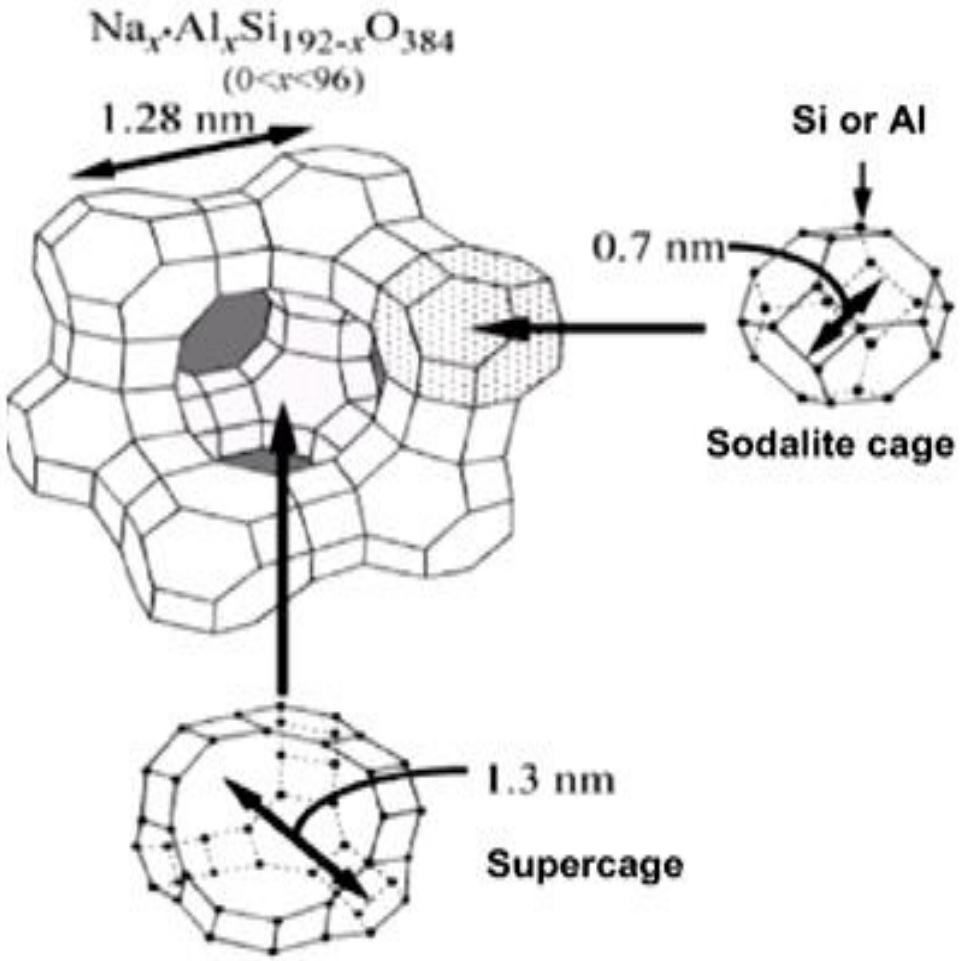

Figure 2.9. The framework structure of zeolite-Y and its micropore system and dimension.

2.4.3. Characterization of Metal Nanoparticles

Finke states that ‘’Many researchers continue to work with compositionally poorly characterized nanoclusters leading to nanoclusters of unknown composition’’ [74]. Characterization of nanoparticles is of vital importance in order to understand particle size and surface composition of nanoparticles. The ultimate goal of the nanoparticle characterization should be look at the surface atom by atom, and under reaction conditions. All the properties cannot be measured with a single method. Different characterization methods give different information about properties of nanoparticles. In order to have a careful analysis of nanoparticles application of several complementary characterization methods is truly needed.

Characterization measurements generally based on: *(i)* specific surface area, *(ii)* specific porosity, *(iii)* pore shape, *(iv)* pore size distribution, *(v)* mean pore size, *(vi)* shapes and size of agglomerates of particles, and *(vii)* particle size distribution [75]. Figure 2.14 represents a scheme from which characterization techniques can be derived. Those techniques based on some type of excitation, shown in inward arrows, and the information that the sample responds is shown in outward arrows.

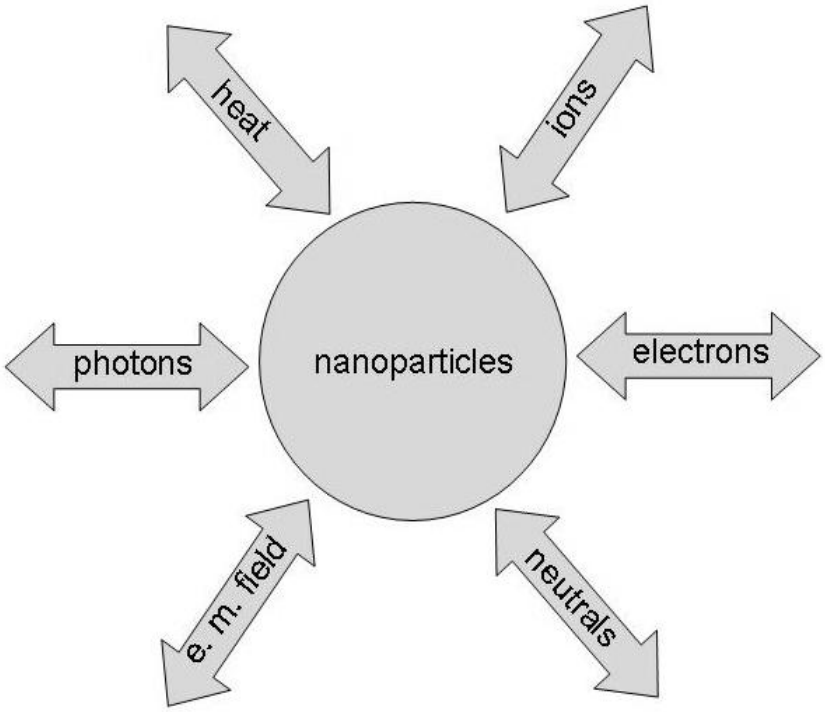

Figure 2.10. Diagram from which most characterization techniques can be derived.

There are several ways of characterization methods but mostly used ones are: transmission electron microscopy (TEM) and or high resolution transmission electron microscopy (HRTEM), scanning electron microscope (SEM), X-ray diffraction (XRD), UV–Visible spectroscopy (UV–VIS), nuclear magnetic resonance spectroscopy (NMR), infrared spectroscopy (IR), elemental analysis, and energy dispersive spectroscopy (EDS). Other less common methods and methods based on target characterization are listed in Figure 2.11.

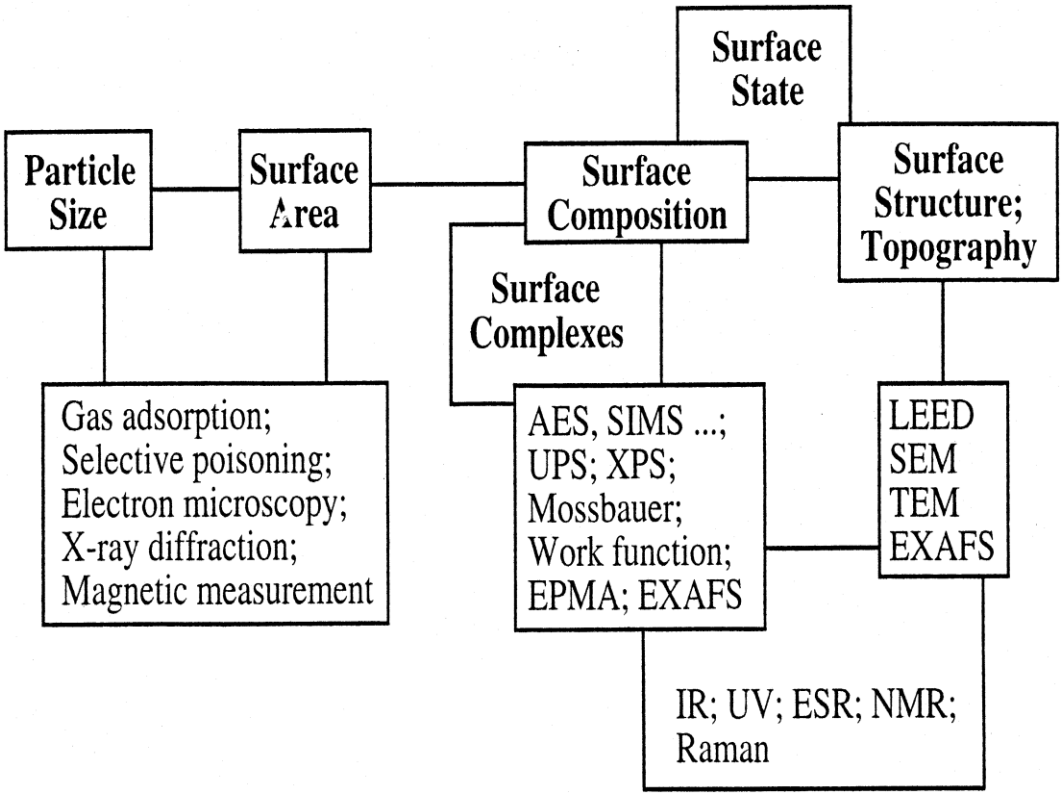

Figure 2.11. Methods for characterization of nanoclusters (adopted from literature [76]).

CHAPTER 3

EXPERIMENTAL

3.1. Materials

Rhodium(III) chloride trihydrate ($RhCl_3 \cdot 3H_2O$), sodium zeolite-Y (NaY zeolite with Si/Al = 2.5), ammonia borane ($H_3N \cdot BH_3$, 97%), sodium borohydride ($NaBH_4$, 98%), D_2O and $BF_3 \bullet (C_2H_5)_2O$ and methanol (MeOH, 99.5%) were purchased from Aldrich. Methanol was distilled over Mg, and then transferred into a nitrogen atmosphere drybox before use. Deionized water was distilled by water purification system (Milli-Q system). All glassware and Teflon coated magnetic stir bars were cleaned with acetone, followed by copious rinsing with distilled water before drying in an oven at 150 °C. All reactions and manipulations were performed under an atmosphere of dry nitrogen using standard Schlenk techniques or in a Labsconco glovebox filled with dry nitrogen unless otherwise specified.

3.2. Preparation of Rhodium(0) Nanoclusters Entrapped in Zeolite-Y

Zeolite-Y was slurried with 0.1 M NaCl to remove sodium defect sites, washed until free of chloride and calcinated in dry oxygen at 500 °C for 12 h before to use. Zeolite confined rhodium(0) nanoclusters were prepared by following a two step procedure; *(i)* In the first step, rhodium(III) cations were introduced into the zeolite-Y by ion exchange of 1000 mg zeolite-Y in 100 mL aqueous solution of 10.2 mg $RhCl_3 \cdot 3H_2O$ (for 0.48 % wt loading) for 72 h at room

temperature. The sample was then filtered by suction filtration using Whatman-1 filter paper, washed three times with 20 mL of deionized water and the remnant was dried in vacuum, *(ii)* in the second step, the solid remnant was added into 100 mL $NaBH_4$ solution (568 mg, 150 mM) at room temperature. Rhodium(III) ion was reduced and the rhodium(0) nanoclusters were formed; the reduction was considered to be complete when no more hydrogen evolution was observed. The zeolite confined rhodium(0) nanoclusters sample was filtered again by suction filtration using Whatman-1 filter paper, washed three times with 20 mL of deionized water, and dried under N_2 gas purging at room temperature for 24 hours, then transferred into the drybox (0_2 < 5 ppm, H_2O < 1 ppm).

3.3. Dehydration of Zeolite Confined Rhodium(0) Nanoclusters

The zeolite confined rhodium(0) nanoclusters powders were placed into a quartz tube whose one-side vacuum (10^{-4} Torr) connected and located in furnace. Thus the sample powders were dehydrated with the following schedule, using a Protek series temperature controller: 0.5 h from 25 to 100°C, 1 h at 100°C, 4 h from 100 to 550 °C and 4 h at 550 °C. After thermal treatment the samples inside the quartz tube were cooled down to room temperature, then sealed and transferred into the glove box (0_2 < 5 ppm, H_2O < 1 ppm). The level of dehydration was checked by complementary Mid-IR spectroscopy. The degree of dehydration was judged by the flatness of the baseline in the ν(OH) stretching and δ (OH) deformation regions, 3400-3700 and 1600-1650 cm^{-1}, respectively, and was found to be complete in all cases [77]. The dehydrated samples were stored in closed nitrogen filled Schlenk tube in the drybox (0_2 < 5 ppm, H_2O < 1 ppm). For all the tests reported hereafter, the zeolite confined rhodium(0) nanoclusters are in dehydrated form unless otherwise stated.

3.4. General Procedure for Testing the Catalytic Activity of Zeolite Confined Rhodium(0) Nanoclusters in the Methanolysis of Ammonia-Borane

The catalytic activity tests of the zeolite confined rhodium(0) nanoclusters in the methanolysis of ammonia-borane were performed in a Fischer-Porter (F-P) pressure bottle connected to a line through Swagelock TFE-sealed quick connects and to an Omega PX-302 pressure transducer interfaced through an Omega D1131 digital transmitter to a computer using the RS-232 module as described elsewhere [70]. The progress of an individual methanolysis reaction was followed by monitoring the increase in the pressure of H_2 gas on LabVIEW 8.0 program. The catalytic activity of zeolite confined rhodium(0) nanoclusters were determined by measuring the rate of hydrogen generation. In a typical reaction 20.6 mg powder of zeolite confined rhodium(0) nanoclusters (with 0.1 wt % Rh; 2×10^{-4} mmol Rh) was weighted in a dry-box and transferred into F-P pressure bottle containing a new $^{5}/_{16}$ in $\times$ $^{5}/_{8}$ in. Teflon coated magnetic stir then brought outside the drybox and placed inside a constant temperature circulating water bath. Next, the F-P bottle was attached to the line (which had already been evacuated for at least 30 min to remove any trace of oxygen and water present) via its TFE-sealed Swagelock Quick-Connects and under nitrogen purging (14 mL dry N_2 / sec) 10 mL of 50 mM $H_3N{\bullet}BH_3$ solution in dry methanol (by dissolving 16 mg $H_3N{\bullet}BH_3$ in 10 mL dry methanol) was added into the F-P pressure bottle rapidly via tap of bottle by using 10 mL pyrex volumetric pipette. The pressure inside the F-P bottle was monitored on PC using LabVIEW 8.0 program. When the pressure inside the F-P bottle established the constant value the reaction was started (t = 0 min.) by stirring the mixture at 900 rpm. When no more hydrogen generation was observed, the experiment was stopped and the F-P bottle was sealed, disconnected from the line and H_2 pressure was released. Then F-P bottle was transferred back into the drybox, a 9 in. glass Pasteur pipette was used to withdraw a ca. 0.5 mL aliquot from the culture tube. This reaction solution aliquot was then added to 1 g of $CDCl_3$ in an individual glass ampule, mixed under agitation using the Pasteur pipette then transferred into a quartz NMR sample tube

(Norell S-500-QTZ) which was subsequently sealed and then brought out of drybox. The ^{11}B NMR spectrum of this solution showed that $H_3N{\bullet}BH_3$ (^{11}B-{^{1}H} = -24 ppm, q) is completely converted to $[H_4NB(OMe)_4]$ (^{11}B-{^{1}H} = 8.6 ppm, s).

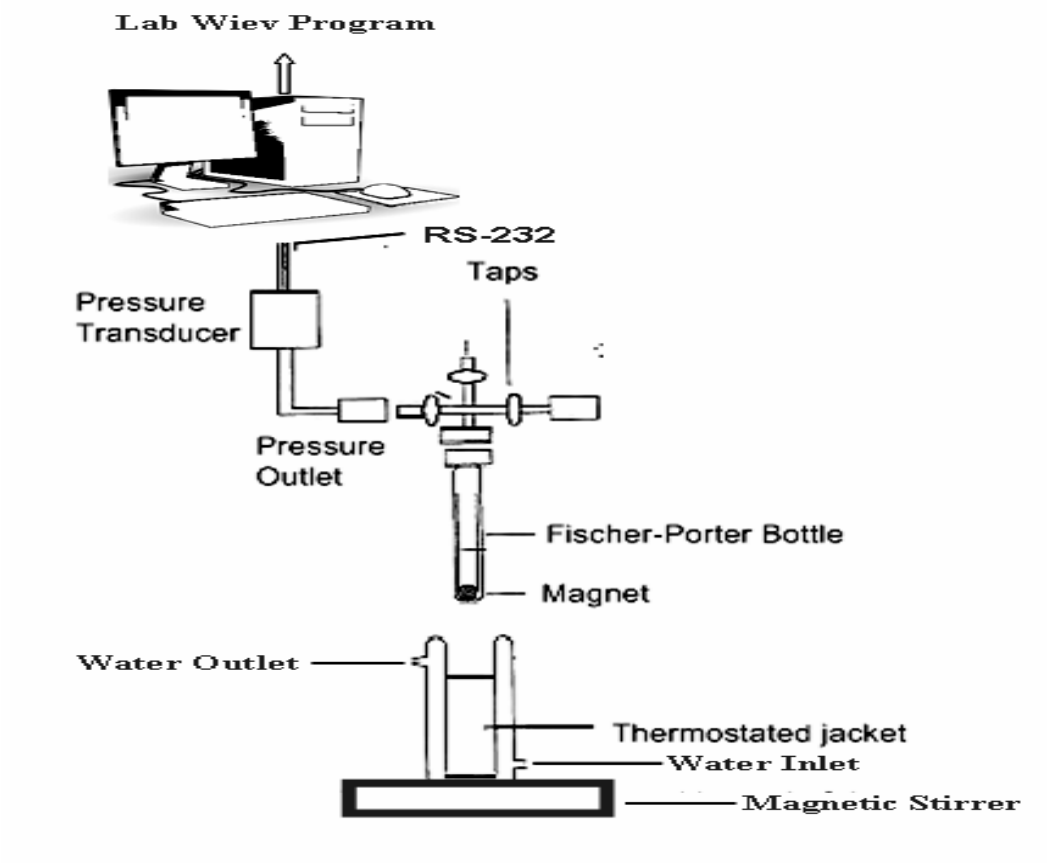

Figure 3.1. The experimental setup used in performing the catalytic methanolysis of ammonia borane and measuring the hydrogen generation rate.

3.5. Control Experiment (1): Self Methanolysis of Ammonia-Borane at Different Temperatures

In a series of experiments at different temperatures (15, 20, 25, 30, 35, 40 °C) in order to determine the rate of the self methanolysis of ammonia-borane in the absence of catalyst, 0.5 mmol (16 mg) $H_3N{\bullet}BH_3$ was dissolved in 10 mL dry methanol and transferred into F-P pressure bottle containing a new $^5/_{16}$ in × $^5/_8$ in. Teflon coated magnetic stir then brought outside the drybox and placed inside a constant temperature circulating water bath. Next, the F-P bottle was attached to the line (which had already been evacuated for at least 30 min to remove any trace of oxygen and water present) via its TFE-sealed Swagelock Quick-Connects. The experiment was started by closing the FP bottle and turning on the stirring at 1000 rpm simultaneously.

3.6. Control Experiment (2): $Na_{56}Y$ Catalyzed Methanolysis of Ammonia-Borane at Different Temperatures

To investigate the effect of the host material zeolite-Y on the catalytic activity of zeolite confined rhodium(0) nanoclusters, the methanolysis of ammonia-borane (50 mM $H_3N{\bullet}BH_3$ in 10 mL dry methanol) was performed in the presence of 408 mg zeolite-Y (corresponds to maxiumum amount of Zeolite-Y that used as a host material for all tests reported here) at 25 ± 0.1 °C by following the same method as given in the section of General Procedure for Testing the Catalytic Activity of Zeolite Confined Rhodium(0) Nanoclusters in the Methanolysis of Ammonia-Borane. Additionally, the same experiment was repeated at different temperatures (20, 30, 35, 40 and 45 °C). It was found that the host material zeolite-Y provides hydrogen generation rates of 0.0125, 0.013, 0.0141, 0.020, 0.022 mL H_2 / sec at 20, 25, 30, 35, 40 and 45°C. All results reported hereafter were corrected to the catalytic activity of zeolite-Y, even it shows negligible activity with respect to zeolite confined rhodium(0)

nanoclusters. The pressure values obtained from each experiments were corrected with respect to self and $Na_{56}Y$ catalyzed methanolysis of $H_3N{\bullet}BH_3$ ($P_{corrected} = P_{Rh(0)Y} - P_{NaY}$) at different temperatures (20, 25, 30, 35, 40 and 45 °C).

3.7. Effect of Rhodium Loading on the Catalytic Activity of Zeolite Confined Rhodium(0) Nanoclusters

In a series of experiments the catalytic activity of zeolite confined rhodium(0) nanoclusters ([Rh] = 1 mM) with a various rhodium loading in the range of 0.21-6.4 % wt (0.21, 0.50, 0.91, 1.2, 1.7, 2.1, 2.7, 3.8, 4.6, 6.4 % wt Rh loadings) were tested in the methanolysis of 5 mL of 1 mmol (32 mg) $H_3N{\bullet}BH_3$ solution at 25 ± 0.1 °C. The experiments were performed in the same way as described in the section "General Procedure for Testing the Catalytic Activity of Zeolite Confined Rhodium(0) Nanoclusters in the Methanolysis of Ammonia-Borane". The best catalytic activity was achieved by 0.50 % rhodium loaded intrazeolite rhodium(0) nanoclusters. For all the tests reported hereafter, the rhodium loading used was ≅ 0.50 wt % unless otherwise stated.

3.8. Kinetic Study of The Methanolysis of Ammonia-Borane Catalyzed by Zeolite Confined Rhodium(0) Nanoclusters in Dry Methanol

In order to establish the rate law for catalytic methanolysis of $H_3N{\bullet}BH_3$ using zeolite confined rhodium(0) nanoclusters (with 0.50 % rhodium loading), two different sets of experiments were performed in the same way as described in the section "General Procedure for Testing the Catalytic Activity of Zeolite Confined Rhodium(0) Nanoclusters in the Methanolysis of Ammonia-Borane". In the first set of experiments, the concentration of $H_3N{\bullet}BH_3$ was kept constant at 50 mM (16 mg $H_3N{\bullet}BH_3$ in 10 mL dry methanol) and the rhodium concentration was varied in the range of 0.1, 0.2, 0.4, 0.6, and 0.8 mM (20.6, 41.2, 82.4, 123.6, 164.8 mg of zeolite confined rhodium(0) nanoclusters respectively). In the second set of

experiments, rhodium concentration was held constant at 0.6 mM (123.6 mg of zeolite confined rhodium(0) nanoclusters in 10 mL dry methanol) while the $H_3N{\bullet}BH_3$ concentration was varied in the range of 50, 100, 200, 400 and 800 mM (16, 32, 64, 128, 256 mg $H_3N{\bullet}BH_3$, respectively). Finally, we performed the catalytic methanolysis of $H_3N{\bullet}BH_3$ in the presence of zeolite confined rhodium(0) nanoclusters at constant $H_3N{\bullet}BH_3$ (1.97 M, 94 mg $H_3N{\bullet}BH_3$ in 1.5 mL dry methanol) and rhodium (6.67 mM, 206 mg zeolite confined rhodium(0) nanoclusters) concentrations at various temperatures in the range of 15-40 °C in order to obtain the activation energy (E_a), enthalpy ($\Delta H^{\#}$) and entropy ($\Delta S^{\#}$).

3.9. Isolability, Bottleability and Reusability of Zeolite Confined Rhodium(0) Nanoclusters Catalyst in the Methanolysis of Ammonia-Borane in Dry Methanol

After the first run of methanolysis of 1 M $H_3N{\bullet}BH_3$ (47 mg $H_3N{\bullet}BH_3$ in 1.5 mL dry methanol), catalyzed by 3.6 mM Rh (110 mg zeolite confined rhodium(0) nanoclusters) at 25 ± 0.1 °C, the catalyst was isolated by vacuum (10^{-3} Torr) dried under N_2 gas purging at room temperature. The dried samples of zeolite confined rhodium(0) nanoclusters were weighted and used again in the methanolysis of 1 M $H_3N{\bullet}BH_3$ (47 mg $H_3N{\bullet}BH_3$ in 1.5 mL dry methanol) and the same procedure was repeated two times more (up to 4^{th} run). The results were expressed as percentage of initial catalytic activity of zeolite confined rhodium(0) nanoclusters in the methanolysis of ammonia-borane.

3.10. Determination of The Catalytic Lifetime of Zeolite Confined Rhodium(0) Nanoclusters in The Methanolysis of Ammonia-Borane in Dry Methanol

The catalytic lifetime of zeolite confined rhodium(0) nanoclusters in the methanolysis of ammonia-borane was determined by measuring the total turnover number (TTO). Such a lifetime experiment was started with a 20 mL dry methanol solution containing 8.3×10^{-3} mmol rhodium (171.5 mg zeolite confined rhodium(0) nanoclusters) 4 mmol $H_3N{\bullet}BH_3$ (127 mg $H_3N{\bullet}BH_3$). When the complete conversion is achieved, more $H_3N{\bullet}BH_3$ was added into the F-P bottle under N_2 purging.

3.11. Characterization of Zeolite Confined Rhodium(0) Nanoclusters

3.11.1. ICP-OES (Inductively Coupled Plasma-Optical Emission Spectrometer)

The rhodium content of the zeolite samples was determined by ICP-OES analysis (Leeman-Direct Reading Echelle) after each sample was completely dissolved in the mixture of HNO_3 / HCl (1/3 ratio).

3.11.2. XRD (X-ray Diffraction)

Powder X-ray diffraction (XRD) patterns were recorded with a MAC Science MXP 3TZ diffractometer using Cu Kα radiation (wavelength 1.5406 Å, 40 kV, 55 mA).

3.11.3. TEM (Transmission Electron Microscopy)

Transmission electron microscopy (TEM) was performed on a JEM-2010F microscope (JEOL) operating at 200 kV. A small amount of powder sample was placed on the copper grid of the transmission electron microscope.

3.11.4. SEM (Scanning Electron Microscope)

Samples were examined at magnification between 100 and 400K. Scanning electron microscope (SEM) images were measured using a JEOL JSM-5310LV at 15 kV and 33 Pa in a low-vacuum mode without metal coating.

3.11.5. FT-IR (Fourier Transform Infrared) Spectroscopy

The FT-IR spectra of samples were recorded under N_2 gas purging using Nicolet Magna-IR 750 spectrometer.

3.11.6. EDX (Energy Dispersive X-Ray) Analysis

The elemental analysis was recorded with an energy dispersive X-ray (EDX) analyzer (KEVEX Delta series) mounted on the Hitachi S-800.

3.11.7. XPS (X-Ray Photoelectron Spectroscopy)

The XPS analysis performed on a Physical Electronics 5800 spectrometer equipped with a hemispherical analyzer and using monochromatic Al Kα radiation (1486.6 eV, the X-ray tube working at 15 kV and 350 W) and pass energy of 23.5 eV).

3.11.8. ^{11}B NMR (Nucleic Magnetic Resonance)

^{11}B NMR spectra were recorded on a Bruker Avance DPX 400 with an operating frequency of 128.15 MHz for ^{11}B. CD_3OD and $BF_3 \bullet (C_2H_5)_2O$ were used as a lock and an external reference, respectively. At the end of the methanolysis reaction, the resulting solutions were filtered and the filtrates were collected for ^{11}B NMR analysis.

3.11.9. N_2 Adsorption-Desorption Analysis

The nitrogen adsorption/desorption experiments were carried out at 77 K using a NOVA 3000 series (Quantachrome Instruments) instrument. The sample was outgassed under vacuum at 573 K for 3 h before the adsorption of nitrogen.

CHAPTER 4

RESULTS AND DISCUSSION

4.1. Preparation of Zeolite Confined Rhodium(0) Nanoclusters

The zeolite confined rhodium(0) nanoclusters were prepared by ion-exchange of Rh^{3+} ions with the extra framework Na^{+} cations of zeolite-Y, followed by reduction of the Rh^{3+} ions in the cavities of zeolite-Y with sodium borohydride in aqueous solution all at room temperature then dehydration by heating from room temperature to 550 °C under 10^{-4} Torr vacuum. Following this three steps procedure, zeolite-Y is first added to the aqueous solution of rhodium(III) chloride in the amount corresponding to the degree of ion exchange and the suspension is stirred for three days at room temperature. After filtering, copious washing with water, and drying in vacuum at room temperature, Rh^{3+}-exchanged zeolite-Y sample was obtained. Next, the Rh^{3+}-exchanged zeolite-Y was reduced by sodium borohydride in aqueous solution yielding zeolite confined rhodium(0) nanoclusters. Then, the powders of the zeolite confined rhodium(0) nanoclusters were dehydrated with the following schedule, using a series temperature controller under 10^{-4} Torr vacuum: 0.5 h from 25 to 100°C, 1 h at 100°C, 4 h from 100 to 550 °C and 4 h at 550 °C.

4.2. Characterization of Zeolite Confined Rhodium(0) Nanoclusters

Zeolite confined rhodium(0) nanoclusters, dehydrated at 550 ^{0}C in vacuum, were characterized by X-Ray diffraction (XRD), X-Ray Photoelectron Spectroscopy (XPS), Transmission Electron Microscopy (TEM), Scanning Electron Microscope (SEM), SEM-EDX, and ICP-OES .

4.2.1. XRD (X-ray Diffraction) Analysis

The XRD patterns of zeolite-Y, Rh^{3+}-exchanged-zeolite-Y and zeolite confined rhodium(0) nanoclusters after dehydration are depicted altogether in Figure 4.1. As seen from the comparison of XRD patterns for zeolite-Y and Rh^{3+} -exchanged zeolite-Y samples there is no noticeable change in both the intensities and positions of the Bragg peaks, indicating that neither the crystallinity nor the lattice of zeolite-Y is essentially altered by ion exchange. Next, the Rh^{3+} exchanged zeolite-Y was reduced by sodium borohydride in aqueous solution yielding zeolite confined rhodium(0) nanoclusters and dehydrated by gradual heating under vacuum. The comparison of XRD pattern of zeolite confined rhodium(0) nanoclusters with those of zeolite-Y and $Rh3^{+}$-exchanged zeolite-Y samples clearly shows that the incorporation of rhodium(III) ion into zeolite-Y and the reduction of rhodium(III) ion forming the rhodium(0) nanoclusters within the cavities of zeolite-Y and the dehydration of zeolite confined rhodium(0) nanoclusters cause no observable alteration in the framework lattice and no loss in the crystallinity of zeolite-Y. As seen from the comparison of XRD patterns for zeolite-Y and Rh^{3+}-exchanged zeolite-Y (Figure 4.1), there is no noticeable change in both the intensities and positions of the Bragg peaks, indicating that neither the crystallinity nor the lattice of zeolite-Y is altered by ion exchange.

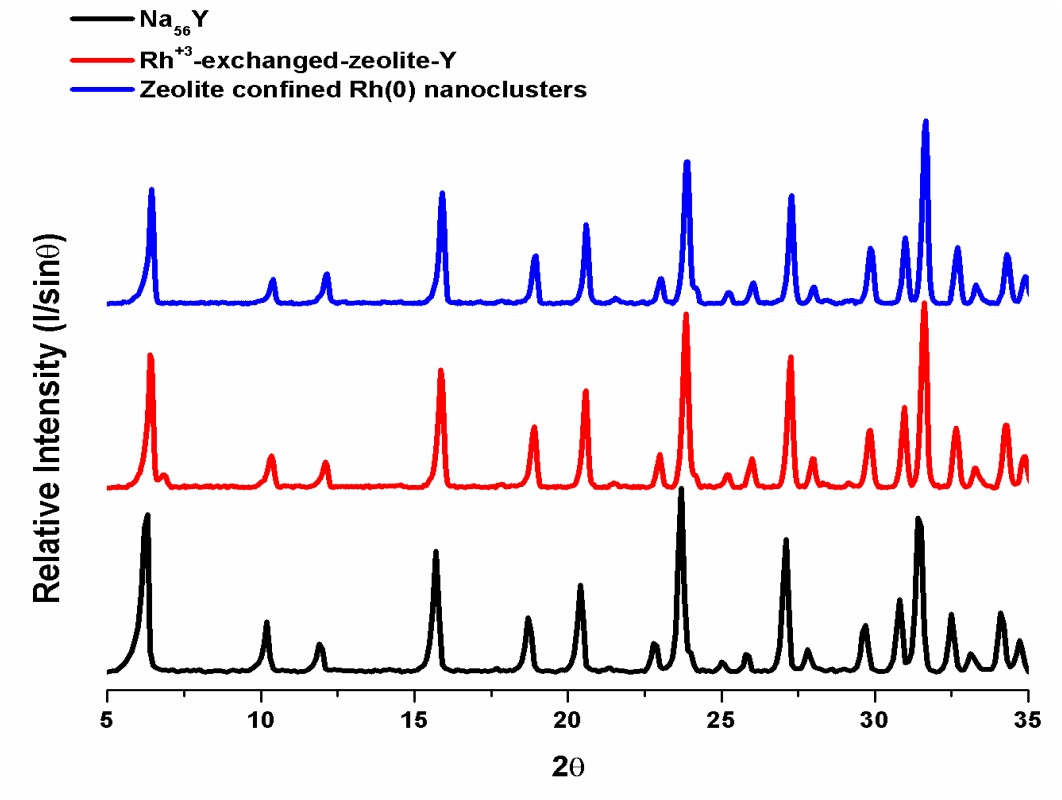

Figure 4.1. The powder XRD patterns of zeolite-Y ($Na_{56}Y$), Rh^{3+}-exchanged zeolite-Y (with a rhodium loading of 0.5 wt %), zeolite confined rhodium(0) nanoclusters prepared from the borohydride reduction of Rh^{3+}-exchanged zeolite-Y and followed by dehydration upon heating to 550 ^{o}C under 10^{-4} Torr vacuum

4.2.2. SEM (Scanning Electron Microscope) and EDX (Energy Dispersive X-ray) Analyse

Figure 4.2 shows the SEM images of zeolite confined rhodium(0) nanoclusters with a metal loading of 0.5 % wt in different magnifications indicating that (*i*) there exist only crystals of zeolite-Y, (*ii*) there is no bulk metal formed in observable size outside the zeolite crystals, (*iii*) the method used for the preparation of zeolite confined rhodium(0) nanoclusters doesn't cause any observable defects in the structure of zeolite-Y, a fact which is also supported by

XRD results. Additionally, SEM modulated EDX confirms (Figure 4.3) that rhodium is, in fact, present in the scanned samples as judged by the $L_{\alpha 1}$ and $L_{\beta 1}$ lines of Rh at 2.69 and 2.80 keV, respectively.[78] This implies that the rhodium metal is within the cavities of zeolite-Y.

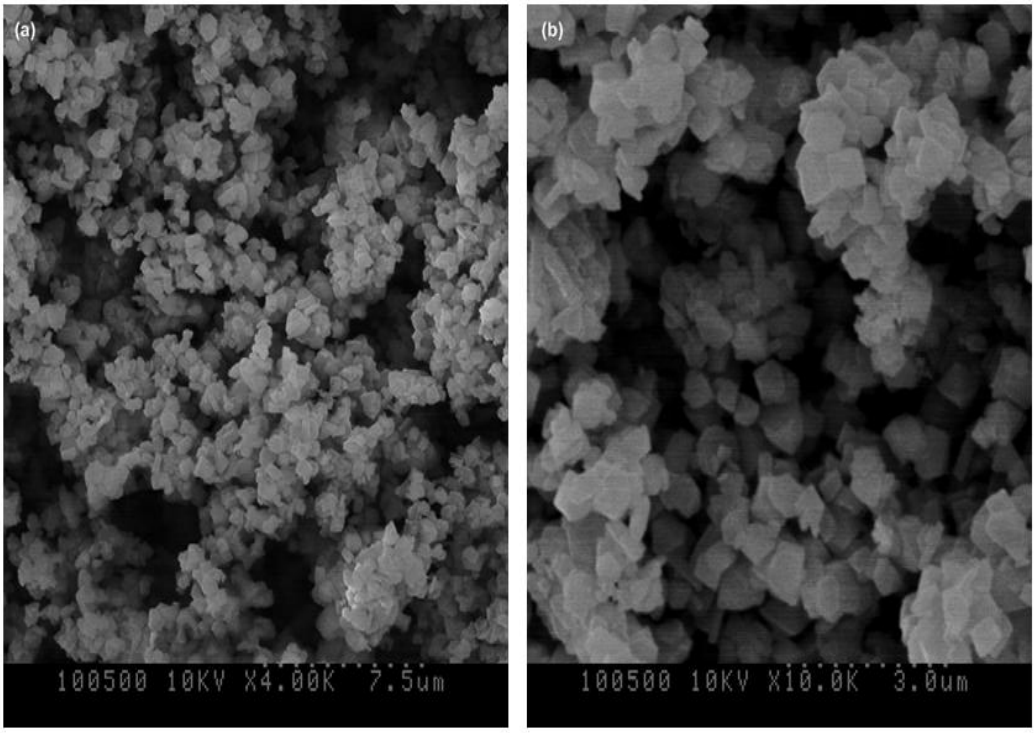

Figure 4.2. The scanning electron microscopy (SEM) images of zeolite confined rhodium(0) nanoclusters with a 0.5 % wt Rh loading (after dehydration process) in different magnificitations. Scale bar (a) 7.5 μm, (b) 3.0 μm

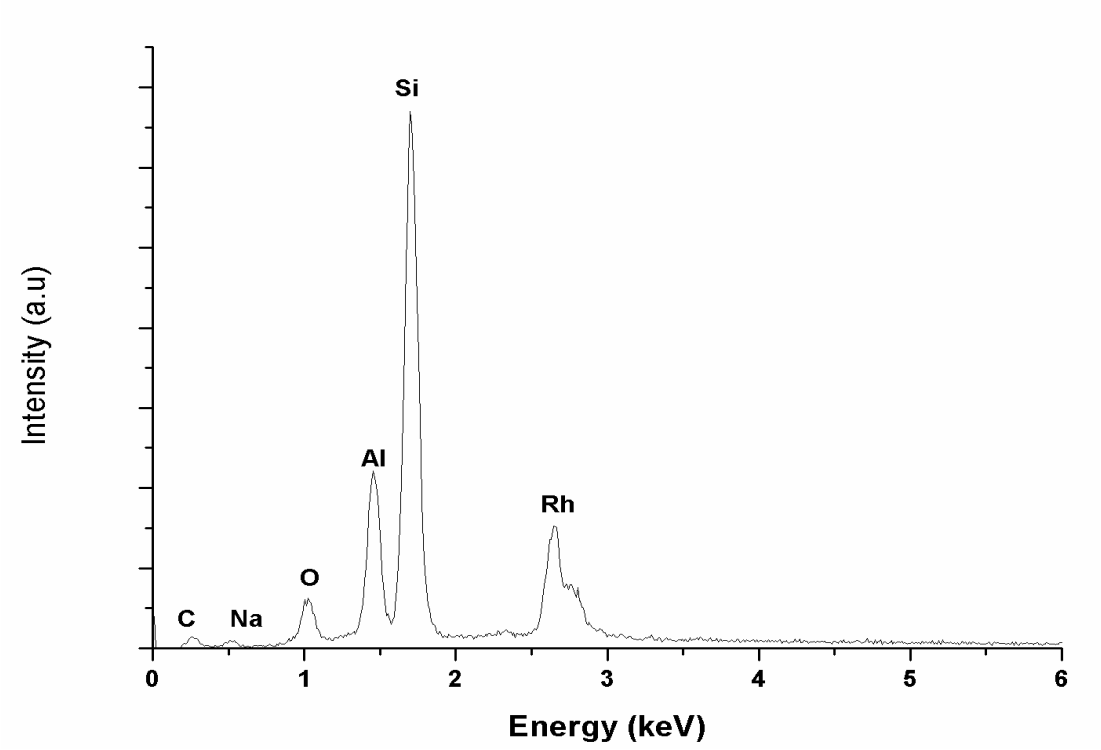

Figure 4.3. EDX analysis of of zeolite confined rhodium(0) nanoclusters with a 0.5 % wt Rh loading (after dehydration process)

4.2.3. TEM (Transmission Electron Microscopy) Analysis

Indeed, the high resolution transmission electron microscopy (HR-TEM) image of the zeolite confined rhodium(0) nanoclusters sample with a rhodium content 0.5 % wt in Figure 4.4 in an arbitrary orientation shows the uniform distribution of rhodium within the highly ordered crystalline structure of zeolite-Y, as evidenced by XRD analysis. Additionally, as also verified by SEM analyses the aggregation of rhodium(0) nanoclusters, which may lead to the blockage of zeolite cages, was not observed from the HR-TEM image of zeolite confined rhodium(0) nanoclusters. Although no bulk rhodium metal is observed outside the zeolite crystals by SEM and TEM, the HRTEM, SEM-EDX and ICP-OES analyses indicate the presence of rhodium in the samples.

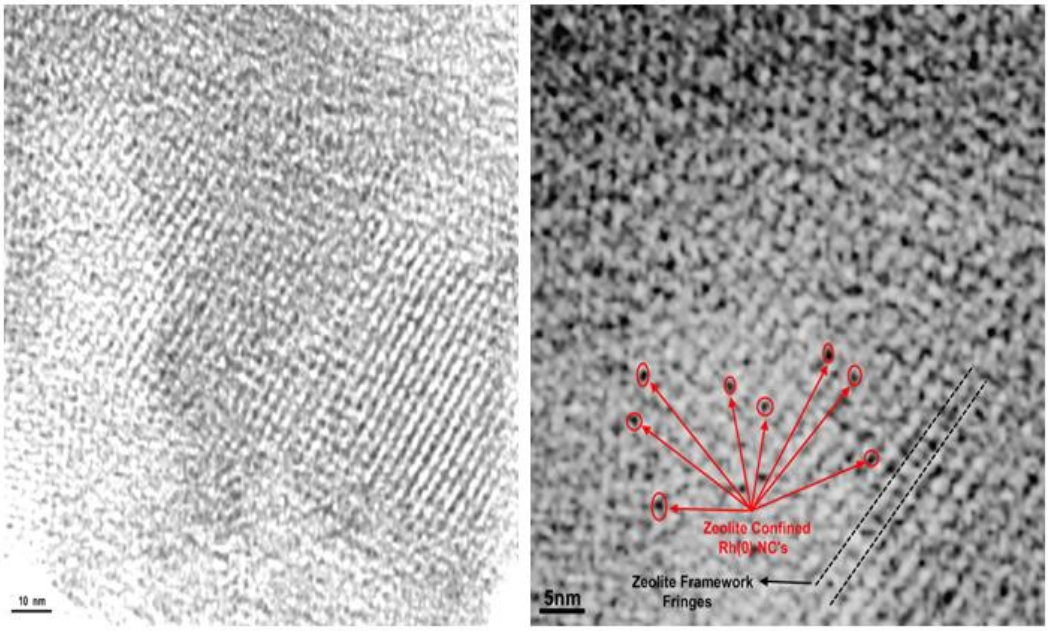

Figure 4.4. High resolution-TEM image of zeolite confined rhodium(0) nanoclusters prepared from the borohydride reduction of Rh^{3+}-exchanged zeolite-Y (with a rhodium loading of 0.5 wt %) and followed by dehydration upon heating to 550 ^{o}C under 10^{-4} Torr vacuum

4.2.4. XPS (X-Ray Photoelectron Spectroscopy) Analysis

The X-ray photoelectron spectrum (XPS) of the zeolite confined rhodium(0) nanoclusters after dehydration process with a rhodium loading of 0.5 % wt is given in Figure 4.5. In addition to zeolite framework elements, it shows two bands at 306.4 and 311 eV readily assigned to Rh(0) $3d_{5/2}$ and Rh(0) $3d_{3/2}$, respectively [79].

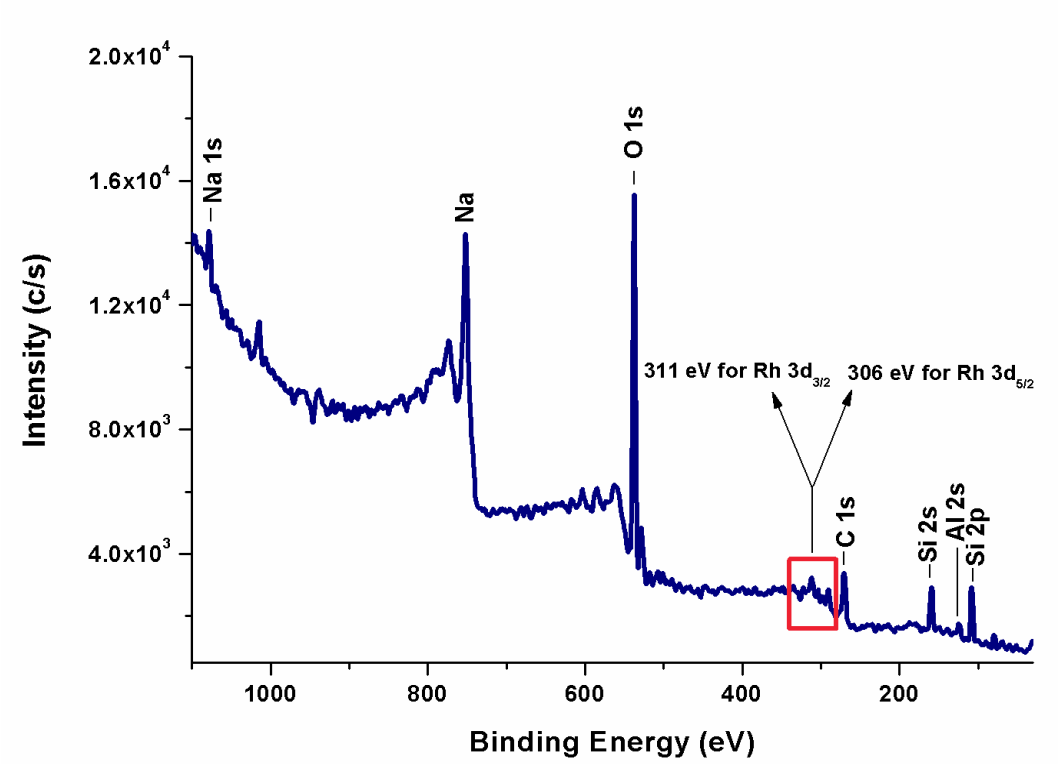

Figure 4.5. X-ray photoelectron spectrum (XPS) of zeolite confined rhodium(0) nanoclusters after dehydration, showing two prominent bands attributed to Rh(0) $3d_{5/2}$ (306.4 eV) and $3d_{3/2}$ (311 eV) peaks.

4.2.5. N_2 Adsorption-Desorption Analysis

Nitrogen adsorption-desorption isotherms of zeolite-Y and zeolite confined rhodium(0) nanoclusters are given in Figure 4.6 and both of them show Type I shape, a characteristic of microporous materials [80]. The micropore volume and area were determined for zeolite-Y and intrazeolite rhodium(0) nanoclusters by *t*-plot method [81]. On passing from zeolite-Y to zeolite confined rhodium(0) nanoclusters, both the micropore volume (from 0.333 to 0.304 cm^3/g) and the micropore area (from 753 to 656 m^2/g) are noticeably reduced.

The remarkable decrease in the micropore volume and micropore area can be attributed to the encapsulation of rhodium(0) nanoclusters in the cavities of zeolite-Y. Furthermore, no hysteresis loop was observed in the N_2 adsorption-desorption isotherm of zeolite confined rhodium(0) nanoclusters indicating that the procedure followed in the preparation of zeolite confined rhodium(0) nanoclusters doesn't create any mesopores.

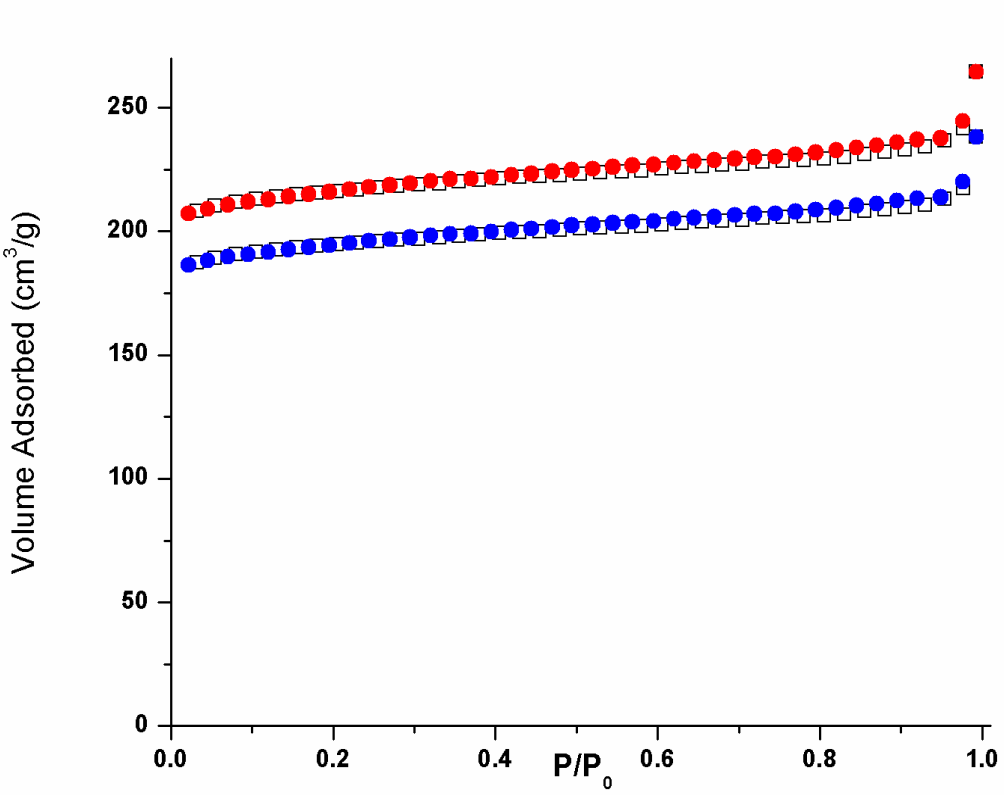

Figure 4.6. N_2 adsorption-desorption isotherms of the host material zeolite-Y (red) and zeolite confined rhodium(0) nanoclusters (blue) with a rhodium content of 0.5 % wt.

4.3. Zeolite-Y ($Na_{56}Y$) Catalyzed Methanolysis of Ammonia-Borane

In the determination of the catalytic activity of zeolite confined rhodium(0) nanoclusters accurately one has to check whether the host material zeolite-Y catalyzes the methanolysis of AB. The methanolysis of AB in the presence of zeolite-Y [82] was performed at various temperatures in the range of 25-45 °C. It was found that the host material zeolite-Y causes hydrogen generation at a rate of 0.0125, 0.013, 0.0141, 0.020, or 0.022 mL H_2 / s at 25, 30, 35, 40 or 45 °C, respectively. The rate of hydrogen generation from the methanolysis of AB in the presence of zeolite-Y increases with the increasing temperature expectedly. Although the methanolysis of AB in the presence of zeolite-Y is slow, all of the catalytic activity results of zeolite confined rhodium(0) nanoclusters in the methanolysis of AB given here were corrected by subtracting the hydrogen gas generated from the methanolysis of AB in the presence of zeolite-Y under otherwise identical conditions.

4.4. Determination of The Effect of Rhodium Loading on the Catalytic Activity of Zeolite Confined Rhodium(0) Nanoclusters

In a series of experiments the catalytic activity of zeolite confined rhodium(0) nanoclusters ([Rh]=1 mM) with a various rhodium loading in the range of 0.21-6.4 % wt (0.21, 0.50, 0.91, 1.2, 1.7, 2.1, 2.7, 3.8, 4.6, 6.4 % wt Rh loadings) were tested in the methanolysis of 5 mL of 1 mmol (32 mg) $H_3N{\bullet}BH_3$ solution at 25 ± 0.1 °C to determine the effect of rhodium loading on the catalytic activity of zeolite confined rhodium(0) nanoclusters. It was found that the zeolite confined rhodium(0) nanoclusters with a rhodium content of 0.5 % wt provided the highest catalytic activity in the methanolysis of ammonia-borane (Figure 4.7).

The reason of different reaction rates with the same rhodium concentration can be explained by the accessibility of substrates to the rhodium(0) nanoclusters in the cages of zeolite-Y. We believe that in the zeolite confined rhodium(0) nanoclusters with a rhodium content of 0.5 % wt most of the rhodium(0) nanoclusters present in the supercage (α-cage), where the substrate molecules can easily access to rhodium(0) nanoclusters with respect to β-cage of zeolite-Y.

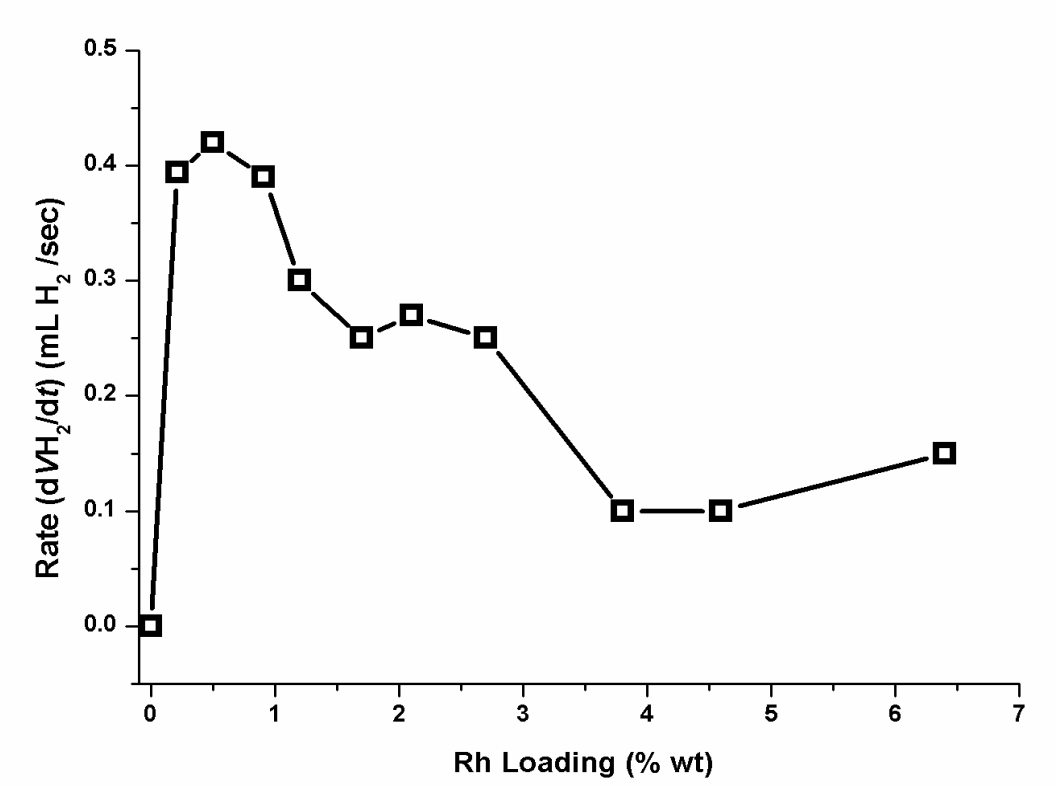

Figure 4.7. The plot of hydrogen generation rate (mL H_2 / s) versus rhodium loadings (in % wt) for the methanolysis of 0.2 M AB solution catalyzed by zeolite confined rhodium (0) nanoclusters ([Rh] = 1 mM) at 25 ± 0.1 °C.

4.5. The Catalytic Activity of Zeolite Confined Rhodium(0) Nanoclusters in the Methanolysis of Ammonia-Borane

The zeolite confined rhodium(0) nanoclusters (with a rhodium content of ≈ 0.5 % wt) were used as catalyst in the methanolysis of AB liberating hydrogen gas. In addition to the volumetric measurement of the hydrogen gas evolution, the completion of methanolysis was ascertained by using ^{11}B NMR spectroscopy. After the reaction, the signal of $H_3N{\bullet}BH_3$ at $\delta = -24.3$ ppm completely disappears and a new resonance at $\delta = 8.3$ ppm shows up, which is readily assigned to the $[B(OMe)_4]^-$ anion. The ^{11}B NMR spectrum are depicted in Figure 4.8.

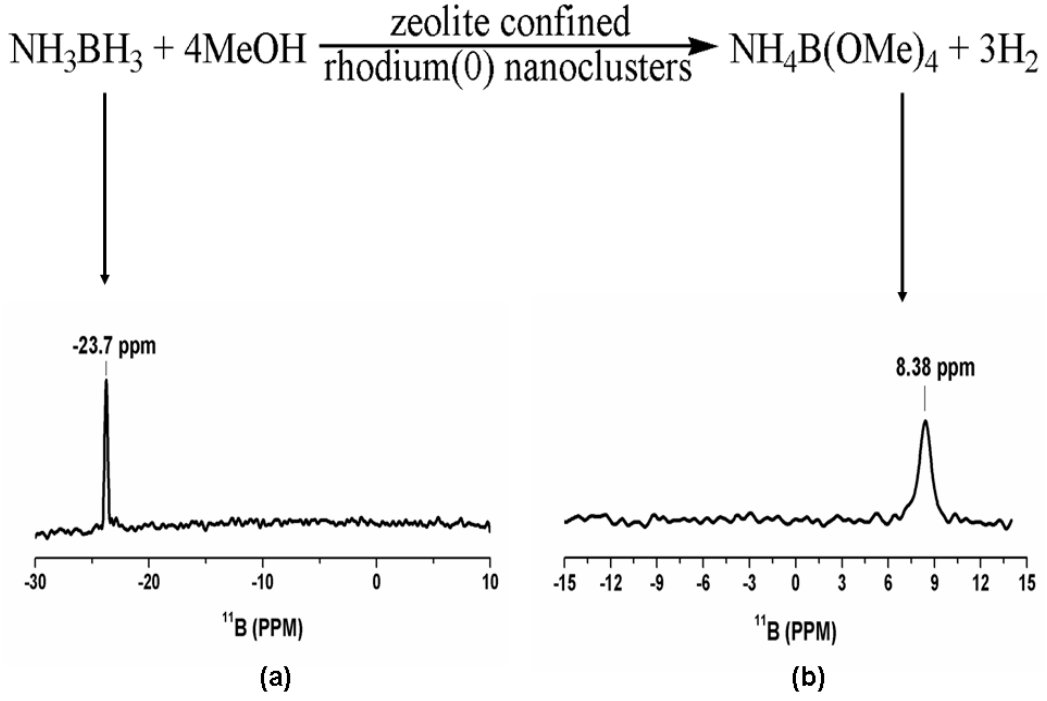

Figure 4.8. (a) ^{11}B NMR spectrum of AB, (b) ^{11}B NMR spectrum of this solution after the completation of methanolysis of AB

4.6. The Rate Law and Activation Parameters of Zeolite Confined Rhodium(0) Nanoclusters in the Methanolysis of Ammonia-Borane

The zeolite confined rhodium(0) nanoclusters were used, for the first time, as catalyst in the methanolysis of ammonia borane. The zeolite confined rhodium(0) nanoclusters were found to be highly active catalyst for the methanolysis of AB as shown in Figure 4.9, which plots the volume of hydrogen generated versus time during the methanolysis of 50 mM AB solution in the presence of zeolite confined rhodium(0) nanoclusters in different concentrations at 25 °C. An almost linear hydrogen evolution starts immediately as the preformed catalyst is used. The hydrogen generation rate was determined from the linear portion of the plot for each experiment with different rhodium concentration. The graph given in Figure 4.10 shows the plot of hydrogen generation rate versus catalyst concentration, both on logarithmic scales. One obtains a straight line, the slope of which is found to be $1.11 \approx 1.0$ within experimental error. This result indicates that the catalytic methanolysis of AB is first order with respect to the rhodium concentration.

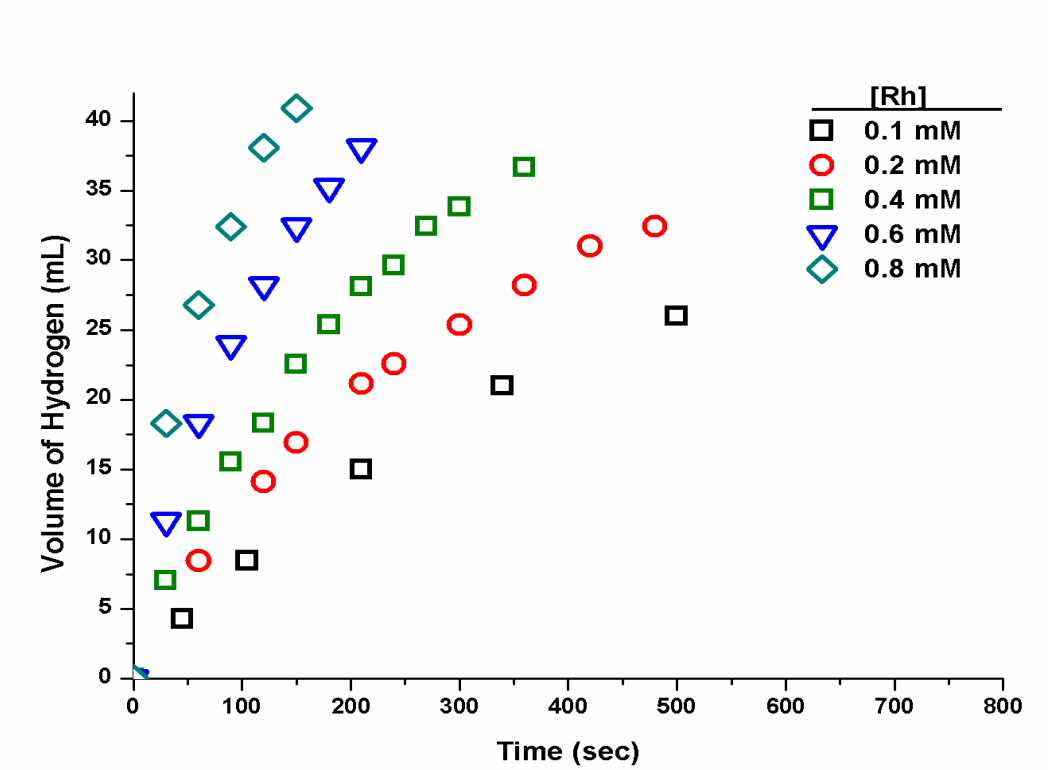

Figure 4.9. Plot of the volume of hydrogen (mL) versus time (s) for the methanolysis of 10 mL of 50 mM AB catalyzed by zeolite confined rhodium(0) nanoclusters with a rhodium content of ≈ 0.5 % wt in different rhodium concentrations at 25.0 ± 0.1 °C.

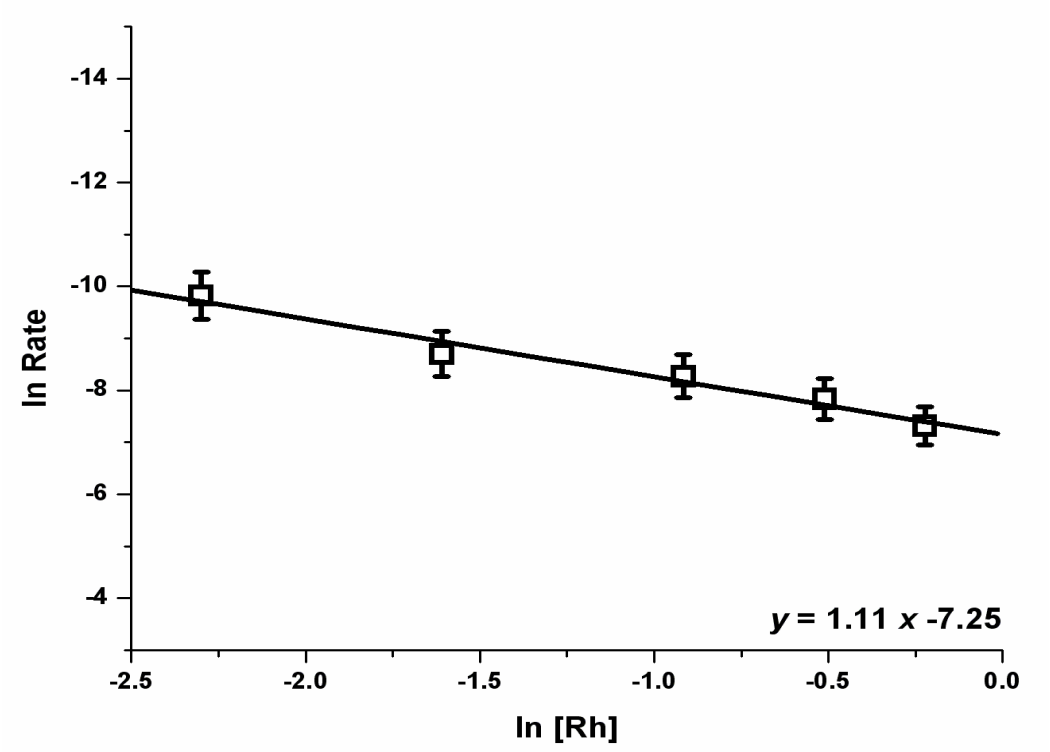

Figure 4.10. The graph of ln (rate) vs ln [Rh] for the zeolite confined rhodium(0) nanoclusters catalyzed methanolysis of ammonia borane, at 25 ± 0.1 ^{0}C.

The effect of substrate concentration on the hydrogen generation rate was also studied by performing a series of experiments starting with varying initial concentration of AB while keeping the catalyst concentration constant at 0.6 mM Rh. Figure 4.11 shows the plot of hydrogen volume versus time for various AB concentrations. The hydrogen generation rate determined from the linear portion of the plot for each experiment was plotted against the substrate concentration, both axes on the logarithmic scale, as given in Figure 4.12. The slope of the straight line is almost zero indicating that the catalytic methanolysis is zero order with respect to substrate concentration.

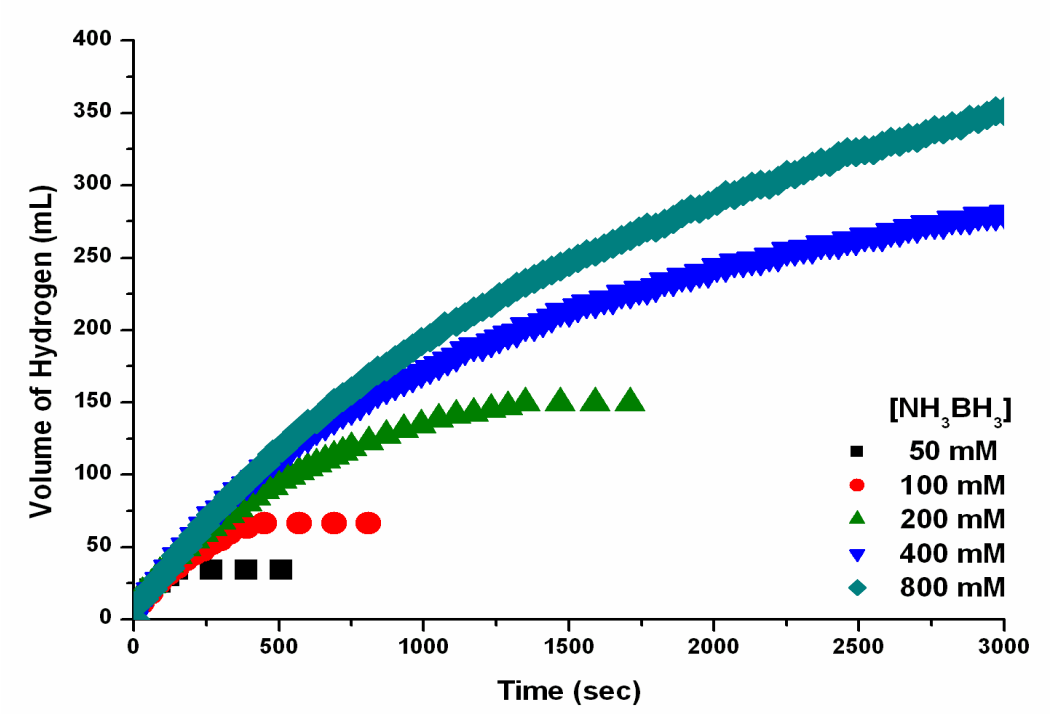

Figure 4.11. Plot of the volume of hydrogen versus time for the methanolysis of AB in various concentration catalyzed by zeolite confined rhodium(0) nanoclusters with a rhodium content of ≈ 0.5 % wt ([Rh] = 0,6 mM) at 25.0 ± 0.1 °C

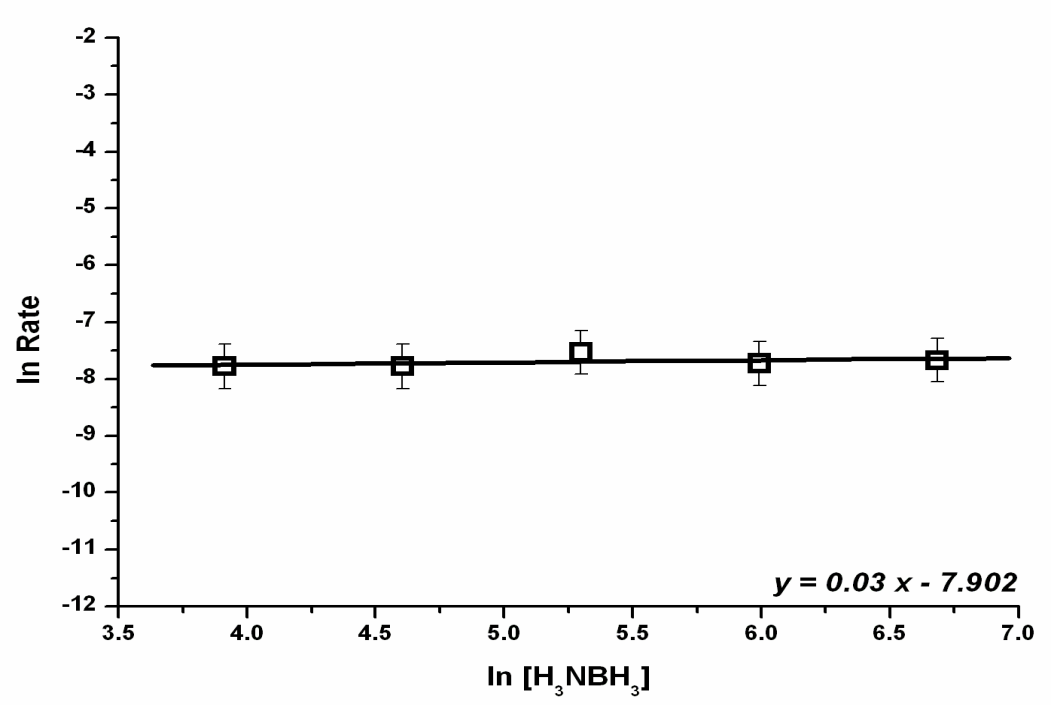

Figure 4.12. The graph of ln (rate) vs ln AB for the zeolite confined rhodium(0) nanoclusters catalyzed methanolysis of ammonia borane 25 ± 0.1 ^{0}C.

It has already been mentioned that kinetics of zeolite confined rhodium(0) nanoclusters catalyzed methanolysis of ammonia borane proceeds first order with respect to Rh concentration and zero order with respect to ammonia borane concentration. Thus, the rate law for the catalytic methanolysis of ammonia borane can be given with the following equation;

$$-\frac{3\mathrm{d}\left[\mathrm{NH_3BH_3}\right]}{\mathrm{d}\,t} = \frac{\mathrm{d}\left[\mathrm{H_2}\right]}{\mathrm{d}\,t} = \mathrm{k}\left[\mathrm{Rh}\right] \qquad (1)$$

In all the experiments, the quantity of ammonia liberation was found to be negligible as expected for the catalyst concentration less than 0.06 mol % and the substrate concentration lower than 6 wt %. The control tests using copper(II) sulfate or acid/base indicator showed no ammonia evolution in detectable amount in all the experiments.

In order to determine activation parameters, the zeolite confined rhodium(0) nanoclusters catalyzed methanolysis of AB was carried out at various temperature in the range of 15-40 °C at constant concentrations of 1.97 M AB and 6.67 mM Rh. The values of rate constant *k* determined from the linear portions of the volume of hydrogen versus time plots at six different temperatures (Figure 4.13). The values of rate constant k are listed in Table 4.1.

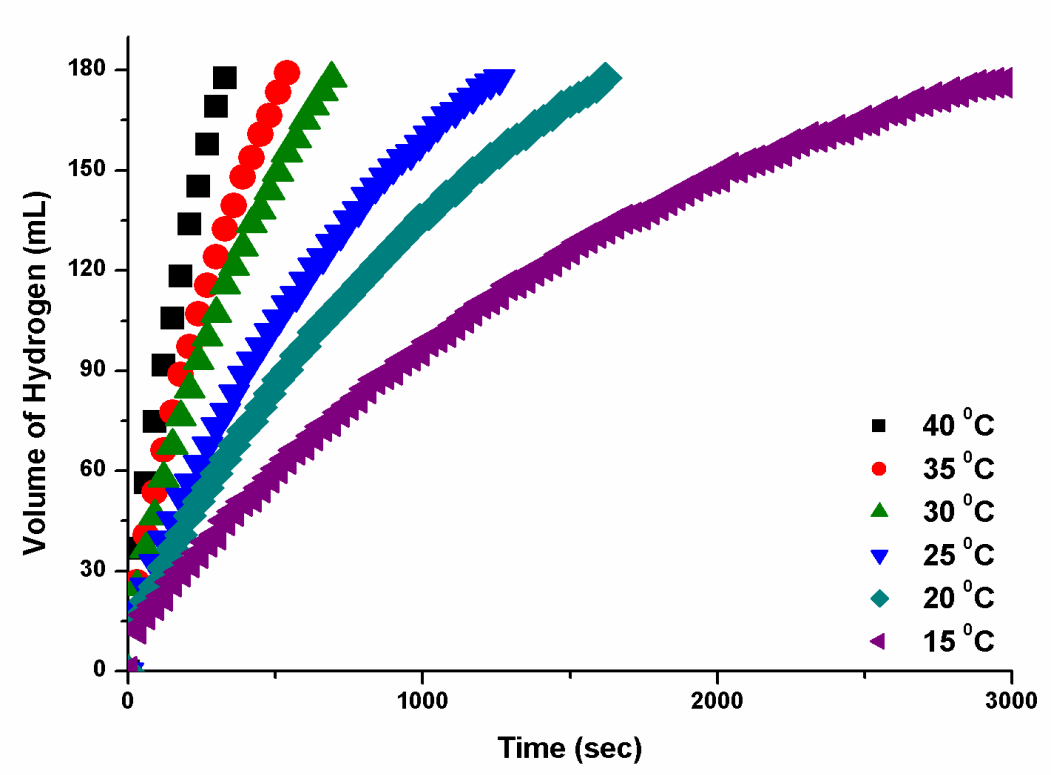

Figure 4.13. Plot of the volume of hydrogen versus time for the methanolysis of AB catalyzed by the zeolite confined rhodium(0) nanoclusters starting with 1.97 M AB and 6.67 mM Rh at different temperatures.

Table 4.1. Rate constants for the zeolite confined rhodium(0) nanoclusters catalyzed methanolysis of ammonia borane

Temperature (^{0}C)	**Rate Constant, *k*,** ([molNH_3BH_3] · [mol Rh(0)]$^{-1}$· s^{-1}
15	0.200
20	0.283
25	0.347
30	0.506
35	0.583
40	0.777

The rate constants were used in the construction of the Arrhenius [83] and Eyring plots [84] given in Figures 4.14 and 4.15, respectively, to calculate the activation parameters. First, the Arrhenius equation was used for the evaluation:

$$k = A\, e^{-Ea / RT} \qquad (2)$$

Where A and Ea are constants characteristics of the reaction and R is the gas constant. Ea is the Arrhenius activation energy and A is the preexponential factor. The natural logarithm of Arrhenius equation gives us;

$$\ln k = \ln A - \frac{Ea}{RT} \qquad (3)$$

The plot of ln k vs $1/T(K^{-1})$ gives a straight line, the slope of which is known as Arrhenius plot and shown in Figure 4.14.

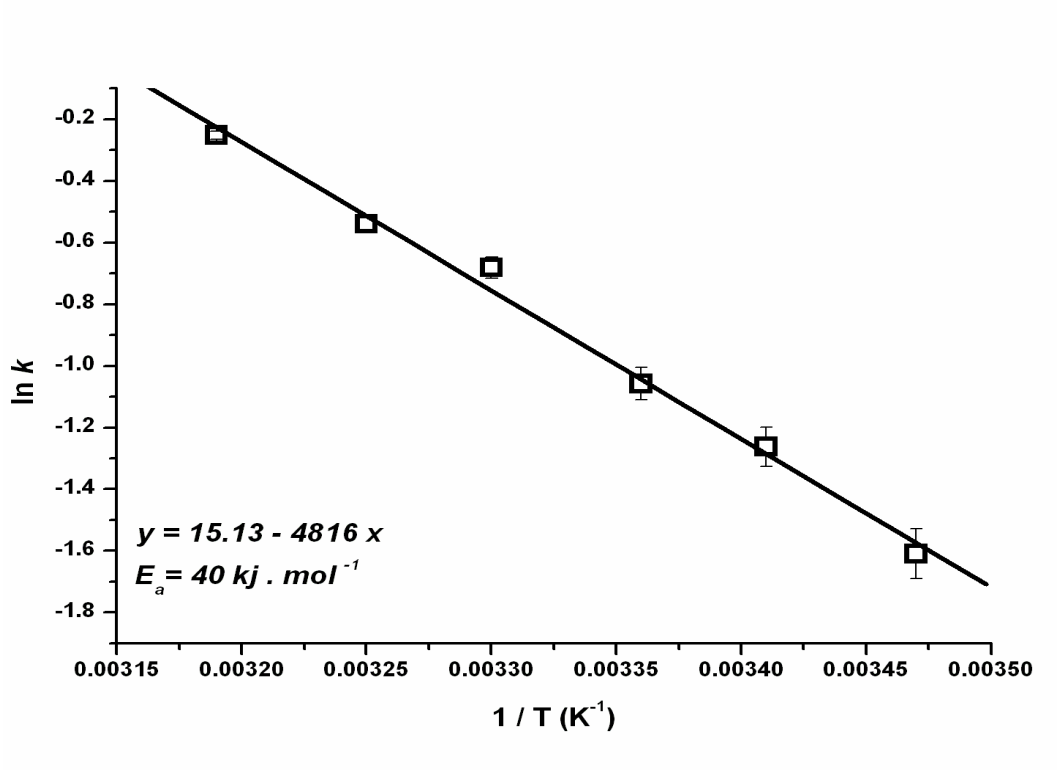

Figure 4.14. Arrhenius plot for the zeolite confined rhodium(0) nanoclusters catalyzed methanolysis of ammonia borane

From the evaluation of Arrhenius plot we get the slope, and the activation energy, *Ea*, for the methanolysis of ammonia borane catalyzed by zeolite confined rhodium(0) nanoclusters catalyzed methanolysis of ammonia borane was calculated as $E_a = 40 \pm 2$ kJ/mol.

Secondly the Eyring equation was used for the evaluation:

$$k = \left(\frac{k_b T}{h}\right) \exp\left(\frac{\Delta S^{\#}}{R}\right) \exp\left(\frac{-\Delta H^{\#}}{RT}\right) \qquad (4)$$

Where k is reaction rate constant, R is gas constant, k_b is Boltzman constant, and h is Planck's constant. $\Delta H^{\neq}$ is the enthalpy of activation and $\Delta S^{\neq}$ is the entropy of activation. The natural logarithm of Eyring equation gives us;

$$\ln\frac{k}{T} = \frac{-\Delta H^{\#}}{R} \cdot \frac{1}{T} + \ln\frac{k_b}{h} + \frac{\Delta S^{\#}}{R} \qquad (5)$$

The enthalpy of activation $\Delta H^{\neq}$ and the entropy of activation were calculated by using Eyring equation and by drawing the graph of ln k/T vs 1/T which is also known as Eyring plot shown in Figure 4.15.

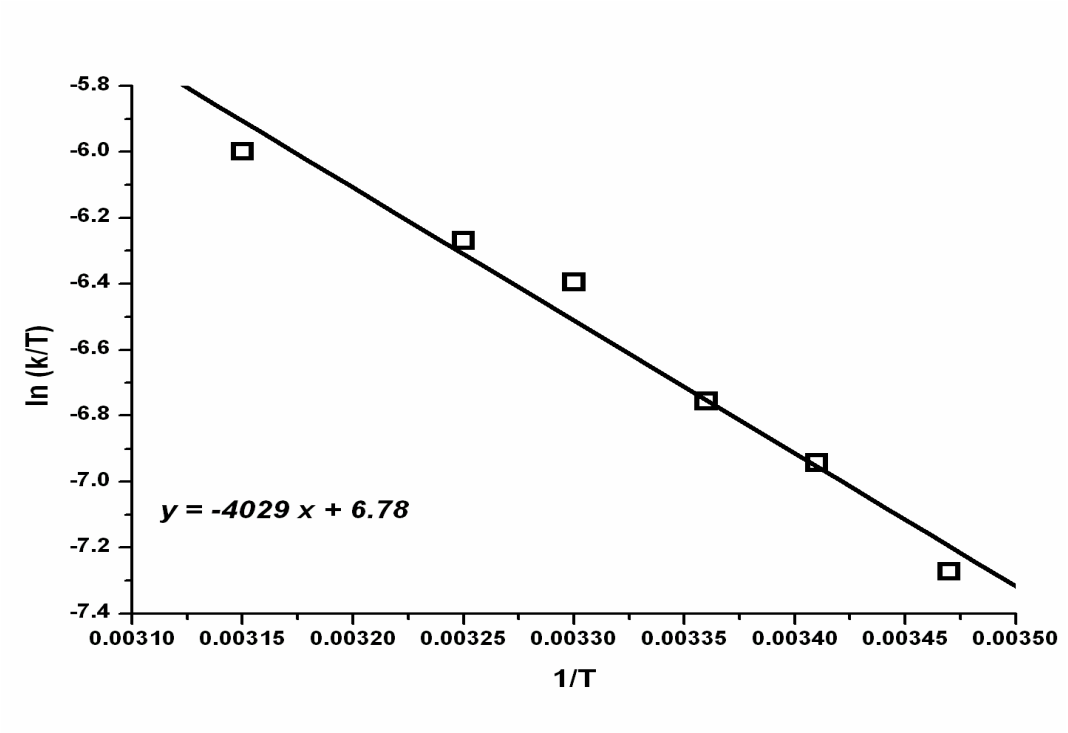

Figure 4.15. Eyring plot for the zeolite confined rhodium(0) nanoclusters catalyzed methanolysis of ammonia borane

From analysis of the Eyring plot, the enthalpy of activation for the zeolite confined rhodium(0) nanoclusters catalyzed methanolysis of ammonia borane was found to be 33 ± 2 kJ/mol, whereas the entropy of activation was found to be $\Delta S^{\neq}$ = -141 ± 5 J/mol.K.

4.7. The Catalytic Lifetime of Zeolite Confined Rhodium(0) Nanoclusters in the Methanolysis of Ammonia-Borane

A catalyst lifetime experiment was started with a 20 mL dry methanol solution containing 8.3×10^{-3} mmol rhodium (171.5 mg zeolite confined rhodium(0) nanoclusters) and 4 mmol $H_3N{\bullet}BH_3$ (127 mg $H_3N{\bullet}BH_3$). It was found that they provide record total turnovers (TTON) of 74300 mol H_2/mol Rh and average turnover frequency (TOF) of 385 mol H_2/mol Rh·h in the methanolysis of ammonia-borane over 193 hours before deactivation (Figure 4.16).

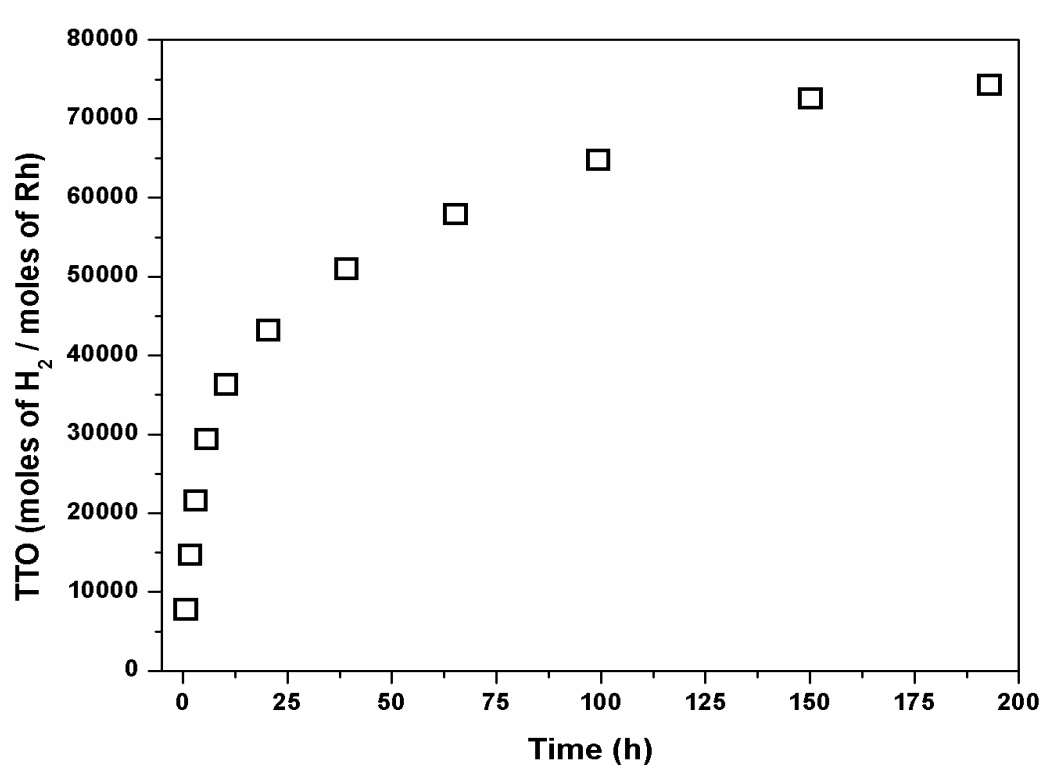

Figure 4.16. Plot of total turnover number (TTO) versus time for the methanolysis of AB catalyzed by the zeolite confined rhodium(0) nanoclusters at 25.0 ± 0.1 °C .

4.8. Isolability, Bottleability and Reusability of Zeolite Confined Rhodium(0) Nanoclusters in the Methanolysis of Ammonia-Borane

Isolability, bottleability and reusability of the zeolite confined rhodium(0) nanoclusters were also tested. After the complete methanolysis of 1 M $H_3N{\bullet}BH_3$ solution catalyzed by zeolite confined rhodium(0) nanoclusters ([Rh] = 3.6 mM) at 25 °C, the catalyst was isolated as black powders by suction filtration, and dried under N_2 purging at room temperature. Black samples of zeolite confined rhodium(0) nanoclusters are bottled under nitrogen atmosphere. The isolated zeolite confined rhodium(0) nanoclusters are redispersible in methanol solution of

ammonia-borane, and yet still active catalyst. Figure 4.17 shows the volume of hydrogen versus time graph up to fourth runs for the zeolite confined rhodium(0) nanoclusters catalyzed methanolysis of ammonia-borane at 25.0 ± 0.1 °C. The zeolite confined rhodium(0) nanoclusters provide complete conversion at the fourth run in the methanolysis of ammonia-borane. This indicates that the zeolite confined rhodium(0) nanoclusters are isolable, bottleable and redispersible and yet catalytically active. In other words, they can be repeatedly used as active catalyst in the methanolysis of ammonia-borane. More importantly, the complete release of hydrogen is achieved in each of the catalytic runs in the methanolysis of ammonia-borane catalyzed by zeolite confined rhodium(0) nanoclusters. The decrease in catalytic activity in subsequent runs may be attributed to the passivation of nanoclusters surface by increasing boron products, e.g. metaborate, which decreases accessibility of active sites [85].

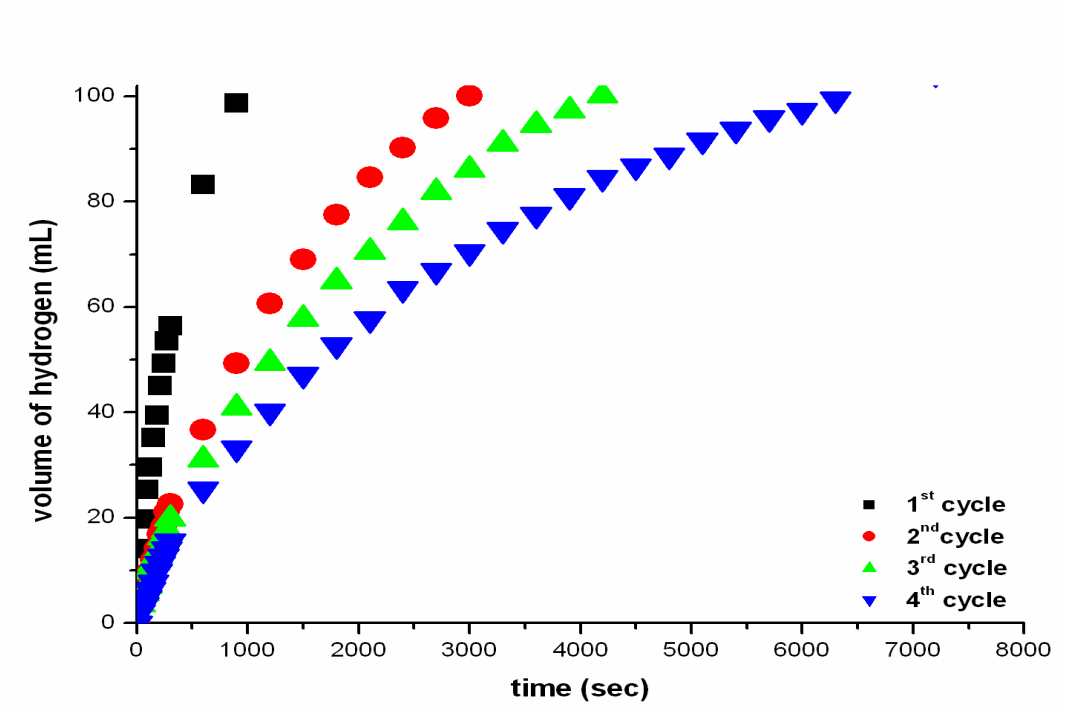

Figure 4.17. The plots of the volume of hydrogen (mL) versus time (s) for the methanolysis of AB catalyzed by the zeolite confined rhodium(0) nanoclusters at 25.0 ± 0.1 °C in successive four runs with complete conversion

CHAPTER 5

CONCLUSIONS

In this study we have demonstrated the use of zeolite confined rhodium(0) nanoclusters as catalyst in the methanolysis of ammonia-borane which has been considered as a promising hydrogen storage material. The results of this study have led the following conclusions and insights;

- Ammonia borane can be used as hydrogen storage material since it provides a safe and practical mean of producing hydrogen at ambient temperature, when zeolite confined rhodium(0) nanoclusters are used as catalyst.

- Hydrolysis of ammonia borane in concentrated solutions can cause ammonia liberation which will hinder its use in fuel cell applications and the hydrolysis product is not recyclable. On the other hand, methanolysis of ammonia borane eliminates both of these problems, by no considerable ammonia liberation and giving a recyclable product as ammoniumtetra-methoxyborate.

- Zeolite confined rhodium(0) nanoclusters are easily prepared at room temperature by ion-exchange of Rh^{3+} ions with the extra framework Na^{+} ions in zeolite-Y, followed by the reduction of the Rh^{3+} ions in the cavities of zeolite-Y with sodium borohydride in aqueous solution.

- The use of metal nanoclusters as catalysts in systems with confined void spaces such as inside mesoporous and microporous solids appears to be an efficient way of preventing aggregation. In this regards zeolite-Y is considered as a suitable host providing highly ordered large cavities (supercages) with a diameter of 1.3 nm.

- Importantly, zeolite confined rhodium(0) nanoclusters has outstanding catalytic activity in the range of 3.12-16.38 mL H_2/min even at low catalyst concentrations (0.10–0.80mM Rh, respectively) and room temperature in the methanolysis of ammonia-borane.

$$NH_3BH_3 + 4MeOH \xrightarrow[Rh(0)\ nanoclusters]{zeolite\ confined} NH_4B(OMe)_4 + 3H_2$$

- The rate law of the methanolysis of ammonia borane catalyzed by zeolite confined rhodium(0) nanoclusters can be given as;

$$-\frac{3d\left[NH_3BH_3\right]}{dt} = \frac{d\left[H_2\right]}{dt} = k\left[Rh\right]$$

- The catalytic methanolysis of ammonia borane proceeds first order with respect to catalyst concentration and zero order with respect to substrate concentration.

- The activation energy (Ea), activation enthalpy ($\Delta H^{\neq}$) and activation entropy ($\Delta S^{\neq}$) of methanolysis of ammonia borane catalyzed by zeolite confined rhodium(0) nanoclusters were found to be 40 ± 2 kJ/mol, 33 ± 2 kJ/mol, and -141 ± 5 J/mol.K, respectively.

- Zeolite confined rhodium(0) nanoclusters provide a record total turnover number (TTO) of 74300 and average turnover frequenct (TOF) of 385 mol H_2/mol Rh·h in methanolysis of ammonia borane at room temperature (Table 5.1).

Table 5.1 Comparison of TOF, TTO, and Ea values of some catalysts and zeolite confined rhodium(0) nanoclusters for the methanolysis of ammonia borane [23].

Catalyst	**Amount of AB and Catalyst**	**TOF (min^{-1})**	**TTO**	**Ea ($kJmol^{-1}$)**
$RuCl_3$	2.9 mmol, 0.03 mol %	173	-	-
$RhCl_3$	2.9 mmol, 2 mol %	101	-	-
$CoCl_2$	2.9 mmol, 2 mol %	3.7	-	-
$NiCl_2$	2.9 mmol, 2 mol %	2.9	-	-
RANEY® Ni	2.9 mmol, 2 mol %	3.6	-	-
Pd/C	2.9 mmol, 2 mol %	2.0	-	-
$PdCl_2$	2.9 mmol, 2 mol %	1.6	-	-
Cu NPs	1 mmol, 15 mol %	0.12	-	-
Cu_2O	1 mmol, 15 mol %	0.21	-	-
Cu–Cu_2O	1 mmol, 15 mol %	0.26	-	-
Co–Co_2B	10 mmol, 20 mol %	7.5	-	-
Ni–Ni_3B	10 mmol, 20 mol %	5.0	-	-
Co–Ni–B	10 mmol, 20 mol %	10.0	-	-
Pd NCs	2 mmol, 0.5 mol %	22.3	23000	35
ZC Rh NCs	4 mmol, 0.21 mol %	385	74300	40

- Moreover, the complete release of hydrogen is achieved even in successive runs performed by redispersing the zeolite confined rhodium(0) nanoclusters isolated after the previous run. Thus, the zeolite confined rhodium(0) nanoclusters are isolable, bottleable and redipersible.

- The superb catalytic activity and the outstandingly long lifetime of zeolite confined rhodium(0) nanoclusters result from; (i) small size of the nanoclusters within the zeolite cages, (ii) the fact that nanoclusters are partially free, since they interact only on one side with internal surface of zeolite. That the channels of zeolite-Y remain open is a propensity of the catalytic reactions, which don't produce any substance blocking the cage apertures of the host material.

- The work reported here clearly shows that: *(i)* in the methanolysis of AB, reducing the particle size of heterogeneous catalyst can provide a significant increase in its activity as the fraction of surface atoms increases with the decreasing particle size, *(ii)* transition metal nanocluster catalysts need to be stabilized to certain extend.

REFERENCES

[1] Orgul, S., Yıldırım, S., Proceedings International Hydrogen Energy Congress and Exhibition IHEC 2005 Istanbul, Turkey, 13-15 July 2005

[2] A Report from the Basic Energy Sciences Advisory Committee, February, **2003,** Office of Sciences, U.S. Department of Energy, www.sc.doe.gov/bes/hydrogen.pdf (24/03/2010).

[3] Annual Energy Outlook 2005 With Projections To 2025, Energy Information Administration, February **2005**, Office of Sciences, U.S. Department of Energy, www.eia.doe.gov/oiaf/aeo/pdf/0383(2005).pdf (24/03/2010).

[4] Marrero-Alfonso E. Y., Beaird A. M., Davis T. A., and Matthews M. A., Industrial & Engineering Chemistry Research, **2009**, 48, 3703–3712

[5] Sherif S.A., Barbir F., Veziroglu T.N., The Electricity Journal, **2005**, 18, 6

[6] Penner S.S., Energy, **2006**, 31, 33–43

[7] (a) Bonner M., Botts T., McBreen J., Mezzina A., Salzano F., and Yang C., International Journal of Hydrogen Energy, **1984**, 9, 4, 269–275, (b) Dutta S., Technology, International Journal of Hydrogen Energy, **1990**, 15, 6, 379–386

[8] Baykara S.Z., Bilgen E., International Journal of Hydrogen Energy, **1989**, 14, 12, 881–889.

[9] (a) Wendt H., Engels H., International Journal of Hydrogen Energy, **1987**, 12, 5, 291–295, (b) Yalcin S., International Journal of Hydrogen Energy, **1989,**14, 8, 551–561.

[10] (a) Bull S.R., Hydrogen Production by Photoprocesses, Proceedings International Renewabe Energy Conference, Honolulu, Hawaii, **1988**, 413–426, (b) Willner I., Steinberger-Willner B., International Journal of Hydrogen Energy, **1988**, 13, 10, 593–604.

[11] National Hydrogen Association, The Hydrogen Technology Assessment, Phase I, Report for NASA, Washington, DC, **1991**

[12] Marbán G., Valdés-Solís T., International Journal of Hydrogen Energy, **2007**, 32, 1625 – 1637

[13] IAC Report, Lighting the Way Towards a Sustainable Energy Futures, Interacademy Council, Amsterdam, **2007**.

[14] Grochala W., Edwards P.P., Chemical Reviews, **2004**, 104, 1283.

[15] Chen P., Xiong Z.T., Luo J.Z., Lin J.Y., Tan K.L. Nature, **2002**, 420, 302.

[16] Bacsa R., Laurent C., Morishima R.; Suzuki H., Lelay M., Journal of Physical Chemistry B, **2004**, 108, 12718.

[17] Lim S.H., Luo J., Zhong Z., Ji W., Lin J., Inorganic Chemistry, **2005**, 44, 4124.

[18] Rood J. A., Noll B.C., Henderson K.W., Inorganic Chemistry, **2006**, 45, 5521.

[19] Marder T., Angewandte Chemie International Edition, **2007**, 46, 8116.

[20] Basic Research Needs Catalysis for Energy, Report from the US Department of Energy, Basic Energy Sciences Workshop Report, August 6-8, Office of Sciences, U.S. Department of Energy, **2007**, www.sc.doe.gov/bes/reports/list.html (24/03/2010).

[21] (a) Stephens F.H., Pons V., Baker R.T., Dalton Transactions, **2007**, 25, 2613; (b) Mohajeri N., Raissi A.T., Adebiyi O., Journal of Power Sources, **2007**,167 482; (c) Stowe A.C., Shaw W.J., Linehan J.C., Schmid B., Autrey T., Physical Chemistry Chemical Physics, **2007**, 9, 1831; (d) Stephens F.H., Baker R.T., Matus M.H., Daniel J., Dixon D.A., Angewandte Chemie International Edition, **2007**, 46 746; (e) Keaton R.J., Blacquiere J.M., Baker R.T., Journal of American Chemical Society, **2007**, 129, 1844.

[22] (a) Chandra M., Xu Q., Journal Power Sources **2006**, 156, 159; (b) Clark T. J., Whittell G. R., Manners I., Inorganic Chemistry, **2007**, 46, 7522; (c) Cheng F., Ma H., Li Y., Chen J., Inorganic Chemistry, **2007**, 46, 788; (d) Chandra M., Xu Q., Journal Power Sources, **2006**, 159, 855; (e) Chandra M., Xu Q., Journal Power

Sources, **2006**, 163, 364; (f) Chandra M., Xu Q., Journal Power Sources, **2007**, 168, 135

[23] (a) Ramachandran V. P., Gagare D. P., Inorganic Chemistry, **2007**, 46, 7810., (b) Caliskan S., Zahmakiran M., Ozkar S., Applied Catalysis B: Environmental, **2010**, 93, 387-394, (c) Kalidindi S. B., Vernekar A. A., Jagirdar B. B., Physical Chemistry Chemical Physics, **2009**, 11, 770-775, (d) Erdogan H., Metin O., Ozkar S., Physical Chemistry Chemical Physics, **2009**, 11, 10519-10525

[24] Ramaswamy A.V., Bulletin of the Catalysis Society of India, **2003**, 2, 140-156

[25] Bond G.C., Catalysis Today, **2002**, 72, 5., (b) Davis R.J., Science, **2003**, 301, 926

[26] Haruta M., Yamada N., Kobayashi T., Iijima S., Journal of Catalysis, **1989**, 115, 301

[27] Hayashi T., Tanaka K., Haruta M., Journal of Catalysis, **1998**, 178, 566

[28] (a) Dimitratos N., Lopez-Sanchez J.A., Morgan D., Carley A., Prati L., Hutchings G.J., Catalysis Today, **2007**, 122, 317., (b) Kanaoka S., Yagi N., Fukuyama Y., Aoshima S., Tsunoyama H., Tsukuda T., Sakurai H., Journal of American Chemical Society, **2007**, 129, 12060., (c) Hughes M.D., Xu Y. J., Jenkins P., McMorn P., Landon P., Enache D.I., Carley A.F., Attard G.A., Hutchings G.J., King F., Stitt E.H., Johnston P., Griffin K., Kiely C.J., Nature **2005,** 437, 1132., (d) Sinha A.K., Seelan S., Tsubota S., Haruta M., Angewante Chemie International Edition, **2004**, 43, 1546.

[29] Grassian V. H., Journal of Physical Chemistry C, **2008,** 112, 18303–18313

[30] Hornstein B. J., Finke R. G., Chemistry of Materials, **2003**, 15, 899-909

[31] Klabunde K. J., Stark J., Koper C., Park D., The Journal of Physical Chemistry, **1996**, 100, 12142.

[32] Aiken III J.D., Lin Y., Finke R.G., Journal of Molecular Catalysis A, **1996**, 114, 29-51.

[33] Ozkar S., Finke R.G., Langmuir, **2003**, 19, 6247-6260.

[34] (a) Jongh L.J.(Ed), Physics and Chemistry of Metal Cluster Compounds, Kluwer Publishers, Dordrect, **1994**, (b) Schmid G. (Ed), Clusters and Colloids: From Theory to Applications, VCH Publishers, New York, **1994.**

[35] Simon U., Schön G., Schmid G., Angewandte Chemie International Edition, **1990**, 248, 1186.

[36] Glanz J., Science, **1995**, 269, 1363.

[37] Antonietti M., Göltner C., Angewandte Chemie International Edition, **1997**, 36, 910

[38] Elghanian R., Storhoff J.J., Mucic R.C., Setinger R.L., Mirkin C.A., Science, **1997**, 277, 1078

[39] Henglein A., Chemical Reviews, **1989**, 89, 1861

[40] (a) G. Schmid, U. Simon, Chemical Communications, **2005**, 6, 697, (b) Schmid G., Advanced Engineering Materials, **2001**, 3, 737.

[41] Colvin V.L., Schlamp M.C., Alivisatos A.P., Nature, **1994**, 370, 354

[42] Sonti S.V., Bose A., Journal of Colloid and Interface Science, **1995**, 170, 575

[43] Vossmeyer T., Delenno E., Heath J.R., Angewante Chemie International Edition, **1997**, 36, 1080

[44] Feldheim D.L., Foss Jr. C.A. (Eds.), Metal Nanoparticles: Synthesis, Characterization, and Applications., Marcel Dekker, New York, **2002**.

[45] Haensel V., *U.S.* Patent, **1949**, 2, 479, 110.

[46] (a) Van Den Berg J. P., Lucien J. P., Germaine G., Thielemans G. L. B., Fuel Processing Technology, **1993**, *35*, 119., (b) Corma A., Martínez A., Martínez-Soria V., Journal of Catalysis, **2001**, *200*, 259.

[47] Bönnemann, G.A. Braun, Angewante Chemie International Edition, **1992**, 35, 1996.

[48] Lewis L.N., Lewis N., Journal of American Chemical Society, **1986**, 108, 7228–7231

[49] Schmidt T.J., Noeske M., Gasteiger H.A., Behm R.J., Britz P., Brijoux W., Bönnemann H., Langmuir, **1997**, 13, 2591

[50] Reetz M.T., Quaiser S.A., Merk C., Chemische Berichte, **1996**, 129, 741-743.

[51] Reetz M.T., Breinbauer R., Wanninger K., Tetrahedron Letters, **1996**, 37, 4499–4502.

[52] Reetz M.T., Lohmer G., Journal of the Chemical Society Chemical Communications, **1996**, 1921–1922

[53] Reetz M.T., Breinbauer R., Wedemann P., Binger P., Tetrahedron, **1998**, 54, 1233–1240

[54] Roucoux A., Schulz J., Patin H., Chemical Reviews, **2002**, 102, 3757-3778

[55] Gaffet E., Tachikart M., El Kedim O., Rahouadj R., Materials Characterization, **1996**, *36*, 1852190

[56] (a) Micheaud C., Mar´ecot P., Gu´erin M., Barbier J., Applied Catallysis:A **1998**, 171, 229, (b) Del Angel P., Dominguez J. M., Del Angel G., Montoya J. A, Lamy-Pitara E., Labruquere S., Barbier S., Langmuir, **2000**, 16, 7210.

[57] Navaladian S., Viswanathan B., Viswanath R. P., Varadarajan T. K., Nanoscale Research Letters, **2007**, 2, 44.

[58] Allmond C. E., Sellinger A. T., Gogick K., Fitz-Gerald J. M., Applied Physics: A, **2007**, *86*, 477

[59] Caruso F. (Ed.:), Grieser F., Ashokkumar M., Colloids and Colloid Assemblies Wiley-VCH: Weinheim, **2004**, p. 120

[60] Evans D. F., Wennerström H., The Colloidal Domain, 2nd ed.; Wiley-VCH: New York, **1999**.

[61] Zahmakıran M., Ozkar S., Journal of Molecular Catalysis A, **2006,** 258, 95-103

[62] Napper D.H., Polymeric Stabilization of Colloidal Dispersions, Academic Press, London, **1983**

[63] Bönnemann H., Braun G., Brijoux W., R., Schulze Tilling A., Seevogel K., Siepen K., Journal of Organometallic Chemistry , **1996**, 520, 143–162.

[64] Metin O., Ozkar S., Journal of Molecular Catalysis A, **2008,** 295, 39-46

[65] Ozkar S., Finke R. G., Journal of American Chemical Society, **2002,** 124, 5796-5810

[66] (a) Schmid G., Pfeil R., Boese R., Bandermann F., Meyers S., Calis G. H. M., Van Der Velden J. W. A., Chemische Berichte **1981**, 114,3634., (b) Amiens C., De Caro D., Chaudret B., Bradley J. S., Mazel R., Roucau C., Journal of American Chemical Society, **1993**, 115, 11638, (c) Duteil A., Schmid G., Meyer-Zaika W., Journal of Chemical Society Chemical Communications, **1995**, 31.

[67] (a) Dassenoy F., Philippot K., Ould Ely T., Amiens C., Lecante P., Snoeck E., Mosset A., Casanove M. J., Chaudret B., New Journal of Chemistry, **1998**, 22, 703, (b) Chen S., Kimura K., Journal of Physical Chemistry B, **2001**, 105, 5397.

[68] (a) Schmid G., Morun B., Malm J. O., Angewante Chemie International Edition English, **1989**, 28, 778., (b) Schmid G., Maihack V., Lantermann F., Peschel S., Journal of Chemical Society Dalton Transactions, **1996**, 589, (c) Schmid G., Emde S., Maihack V., Meyer-Zaika W., Peschel S., Journal of Molecular Catalysis A: Chemical, **1996**, 107, 95

[69] Rodriguez A., Amiens C., Chaudret B., Casanove M. J., Lecante P., Bradley J. S., Chemistry of Materials, **1996**, 8, 1978

[70] (a) Zahmakıran M., Özkar S., Langmuir, **2008**, 24, 7065–7067, (b) Zahmakıran M., Özkar S., Langmuir, **2009**, 25, 2667–2678

[71] (a) Tang Q., Zhang Q., Wang P., Wang Y., Wan H., Microporous and Mesoporous Materials, **2005**, 86, 38-49., (b) Rakap M., Ozkar S., Applied Catalysis B: Environmental, **2009**, 91, 21-29, (c) Zahmakiran M., Durap F., Ozkar S., International Journal of Hydrogen Energy, **2010**, 35, 187-197

[72] Rabo J. A., Zeolite Chemistry and Catalysis, ACS Monograph, Washington, **1976.**

[73] Weitkamp J., Solid State Ionics, **2000**, 131, 175–188

[74] Finke RG (ed.). Synthesis, Characterization and Applications. Marcel Dekker: New York, **2002**

[75] Smith G. V., Notheisz F. , Heterogeneous Catalysis in Organic Chemistry; Academic Press, San Diego, **1999**

[76] Aiken III J.D., Finke R.G., Journal of Molecular Catalysis A: Chemical, **1999**, 145, 1–44

[77] Baker M. D., Godber J., Ozin G. A., Journal of American Chemical Society, **1985**, 107, 3033.

[78] Jones I. P., Chemical Microanalysis Using Electron Beams; The Institute of Materials; London, **1992**.

[79] Mevellec V., Nowicki A., Roucoux A., Dujardin C., Granger P., Payen E.; Philippot K., New Journal of Chemistry, **2006**, 30, 1214.

[80] Storck S., Bretinger H., Maier W. F., Applied Catalysis A., **1998**, 174, 137.

[81] Mikhail R. S. H. , Brunauer S., Bodor E. E., Journal of Colloid and Interface Science, **1968**, 26, 45.

[82] We found that in the presence of hydrated zeolite the reaction shifts to hydrolysis of ammonia-borane even in methanol, which gives tetraborate as a product (11B-NMR chemical shift of 12 ppm).

[83] Laidler K. J., Chemical Kinetics, Third Edition, Benjamin-Cummings, **1997**.

[84] Eyring H., Polanyi M., Zeitschrift für Physikalische Chemie Abteil B, **1931**, 12 , 279.

[85] (a) Jaska C. A., Clark T. J., Clendenning S. B., Grozea D., Turak A., Lu Z-H., Manners I., Journal of American Chemical Society, **2005**, 127, 5116., (b) Clark, T. J.; Whittell, G. R.; Manners, I. Inorg. Chem. **2007**, 46, 7522.

APPENDIX A

KINETIC DATA

Table A.1 Volume of hydrogen (mL) versus time (s) for the methanolysis of 10 mL of 50 mM AB catalyzed by zeolite confined rhodium(0) nanoclusters with a rhodium content of ≈ 0.5 % wt in different rhodium concentrations at 25.0 ± 0.1 °C

Time (s)	0.1 mM	0.2 mM	0.4 mM	0.6 mM	0.8 mM
0	0	0	0	0	0
30			7,05	11,28	18,33
45	4,28				
60		8,46	11,28	18,33	26,79
90			15,51	23,97	32,43
105	8,46				
120		14,1	18,33	28,2	38,07
150		16,92	22,56	32,43	40,89
180			25,38	35,25	40,89
210	15	21,15	28,1	38,07	40,89
240		22,56	29,61	38,07	40,89
270			32,43	38,07	40,89
300		25,38	33,84	38,07	40,89
340	21				
360		28,2	36,66	38,07	40,89
420		31,02	36,66	38,07	40,89
480		32,43	36,66	38,07	40,89
500	26	32,43			
600	26	32,43	36,66	38,07	40,89

Table A.2 Volume of hydrogen versus time for the methanolysis of AB in various concentration catalyzed by zeolite confined rhodium(0) nanoclusters with a rhodium content of ≈ 0.5 % wt ([Rh] = 0.6 mM) at 25.0 ± 0.1 °C

Time (s)	50 mM	100mM	200mM	400mM	800mM
0	0	0	0	0	0
30	14,1	11,28	18,33	11,28	14,1
60	21,15	18,33	23,97	19,74	21,15
90	25,38	25,38	32,43	26,79	28,2
120	29,61	31,02	38,07	35,25	35,2
150	33,84	35,25	43,71	43,71	43,71
300	33,84	54,99	67,68	76,14	77,55
600	33,84	66,27	104,34	125,49	135,36
1200		66,27	145,23	188,94	215,73
1800			149,46	229,83	270,72
2400				259,44	315,84
3000				280,59	351,09
3300				289,05	353,91
3600				294,69	353,91
3900				301,74	353,91
4200				304,56	
4500				308,79	
4800				311,61	
5100				313,02	
5400				315,84	
5700				315,84	
6000				315,84	

Table A.3 Volume of hydrogen versus time for the methanolysis of AB catalyzed by the dehydrated ZC-Rh(0) nanoclusters starting with 1.97 M AB and 6.67 mM Rh at different temperatures (15-40 ^{0}C)

Time (s)	15 ^{0}C	20 ^{0}C	25 ^{0}C	30 ^{0}C	35 ^{0}C	40 ^{0}C
0	0	0	0	0	0	0
30	12,69	15,51	18,33	25,38	26,79	36,66
60	16,92	21,15	25,38	36,66	40,89	56,4
90	19,74	25,38	32,43	46,53	53,58	74,73
120	22,56	31,02	39,48	57,81	66,27	91,65
150	26,79	36,66	45,12	67,68	77,55	105,75
300	40,89	59,22	73,32	107,16	124,08	169,2
600	67,68	97,29	117,03	164,97	188,94	235,47
1200	109,98	150,87	174,84	221,37	234,06	246,75
1800	139,59	184,71	200,22	228,42	235,47	248,16
2400	162,15	203,04	207,27	228,42	235,47	248,16
3000	177,66	207,27	207,27	228,42	235,47	248,16
3300	183,3	207,27				
3600	187,53	207,27				
3900	191,055					
4200	191,055					
4500	191,76					
4800	193,17					
5100	194,58					
5400	195,99					
5700	195,99					
6000	195,99					